Pulse Detonation Engines: Initiation, Propagation, and Performance

a portion of

A Collaborative Multi-University Program of Research on Pulse Detonation Engines

Final Report for Award ONR N00014-02-1-0589

Principal Investigator: J.E. Shepherd

Graduate Aeronautical Laboratories
California Institute of Technology
Pasadena, CA 91125

GALCIT Report FM2005.002

May 23, 2005

Foreword

The work was carried out under the direction of J. E. Shepherd in the Explosion Dynamics Laboratory, part of the Graduate Aeronautical Laboratories at the California Institute of Technology (GALCIT). The research was performed by an extremely talented and hardworking group of graduate and undergraduate students.

Eric Schultz (PhD 00)
Joanna Austin (PhD 03)
Eric Wintenberger (PhD 04)
Tony Chao (PhD 04)
Florian Pintgen (PhD 04)
Scott Jackson (PhD 05)
Marcia Cooper (PhD 04)
Daniel Lieberman (PhD in progress)
Joe Jewell (BS 04)
Marty Grunthaner (BS 03)
Paul Buraczewski

The commitment and close cooperation of this group enabled the study of a very wide range of topics and significant contributions to several aspects of detonation science and pulse detonation engine technology. It was a real pleasure to mentor this group of students and learn together with them. Suzy Dake did an exceptional job of taking care of the administrative details and helping prepare all the manuscripts. My heartfelt thanks to everyone.

Joe Shepherd
Pasadena
May 2005

Abstract

Research carried out from 2003-2005 at the Explosion Dynamics Laboratories at Caltech under an ONR contract has examined many issues critical to Pulse Detonation Engine (PDE) development. These include: detonation structure imaging using OH PLIF; a narrow channel facility for examining regular and irregular detonations; detonation diffraction; mechanism of soot track generation; fundamental and applied studies of detonation initiation; direct measurements and analytical modeling of impulse from a detonation tube, including the effects of partial fill and nozzles; models of detonation engine performance; thermodynamic analysis of unsteady and steady propulsion systems. Each of these aspects of our program is discussed and key results are presented.

Contents

List of Figures

1 Introduction

Research at the Explosion Dynamics Laboratories at Caltech from 1999-2005 has examined many issues critical to Pulse Detonation Engine (PDE) development. These include: fundamental detonation structure measurements; OH PLIF technique development; direct measurements and analytical modeling of impulse from a detonation tube and detonation-based propulsion cycles; the effects of partial fill, entrance, and exit geometry; initiation using shock and detonation wave implosion; initiation using shock focusing; and initiation with turbulent jets and corona discharge.

This report describes some research carried out at the California Institute of Technology from May 1, 2003 until December 31, 2004. The work described was sponsored by the Office of Naval Research under Department of the Navy Grant No. N00014-02-01-0589 as a subaward by Stanford University Contract PY-1905. Only the portion of the work carried out at Caltech is described in this report. A previous report "A Multidisciplinary Study of Pulse Detonation Engine Propulsion" describes the work carried out at Caltech and other institutions under Award ONR N0014-99-1-0744 for the period 30 April 1999 to 10 October 2002.

Our group was part of a larger research program involving the groups of Bob Santoro and Vigor Yang at Penn State, Ron Hanson's group at Stanford, Kailas Kailasanath at NRL, and also Chris Brophy, Dave Netzer, and Jose Sinabaldi at the Naval Postgraduate School. Our work benefited from the exchange of ideas and techniques with all of these groups. The work on corona discharge initiation was done in collaboration with Martin Gunderson's group at USC. Fred Schauer's group at WPAFB provided valuable data on partial fill performance and useful insights into practical engine operation. In addition to our team members and direct collaborators, we were associated with several industrial partners (APRI and GE). In particular, Tony Dean's group at GE Global Research was very supportive during key phases of our work.

As mentioned in the foreword, the actual work was done by the students, working both individually and as teams. The financial support of these students by the Office of Naval Research as facilitated by Gabriel Roy was essential for providing a stable funding base so that we could explore fundamental issues in depth.

2 Detonation Structure

A fundamental understanding of the detonation propagation mechanisms is basic to PDE development as it is highly relevant to the areas of detonation initiation, confinement geometry, and minimum tube size. The detonation structure of mixtures exhibiting a very regular cellular pattern, argon-diluted H_2-O_2, was studied extensively in the past in our laboratory using laser induced fluorescence imaging of the OH radical (Pintgen et al., 2003b,a). With the construction of the new narrow channel facility (Austin, 2003, Grunthaner and Austin, 2003), this work was extended to more irregular mixtures, hydrocarbon-air, which are more relevant to PDE applications. The narrow channel is a high aspect ratio (18×152 mm), rectangular channel (Fig. 1). The channel is 4.2 m long with 184 mm diameter windows approximately 3.6 m downstream of the initiation point.

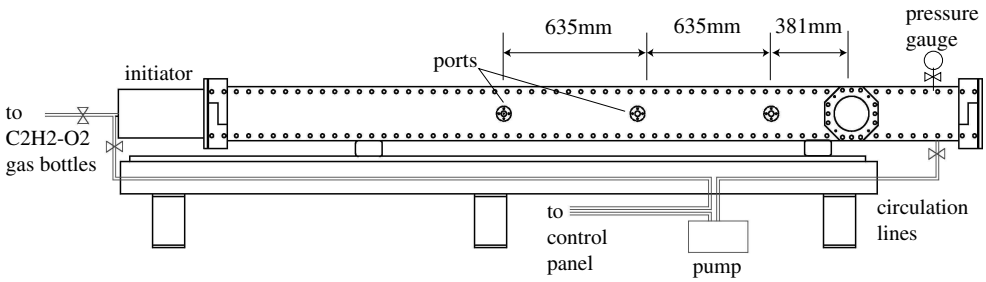

Figure 1: Schematic of the narrow channel facility.

Initiation was by a planar detonation front produced by merging eight smaller wavefronts. Pressure transducers monitored the planarity of the detonation front at the exit plane of the initiator (Jackson and Shepherd, 2002, Jackson et al., 2003). Four pressure transducers were mounted along the channel to measure the detonation pressure and time of arrival. High-speed shadowgraph movies and simultaneous schlieren-PLIF visualization techniques of the OH radical were used. Experimental images of fully developed detonation fronts traveling at the Chapman-Jouguet (CJ) velocity were made for several fuel-oxidizer mixtures. The degree of instability of detonation fronts in different mixtures is evaluated by comparing calculated mixture parameters with the longitudinal neutral stability curve. The images reveal that the structure of the front increases dramatically in complexity for more unstable mixtures (Austin et al., 2005b).

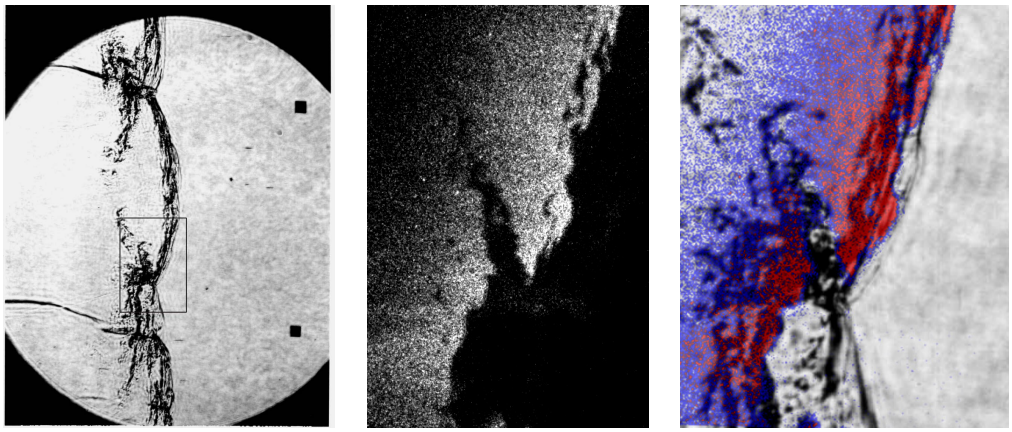

(a) (b) (c)

Figure 2: Images of a detonation front propagating from left to right in C_2H_4-$3O_2$-$10.5N_2$, P_1=20 kPa in the narrow channel. (a) schlieren image. The box shows the location of the corresponding OH fluorescence image shown in (b). (c) Superimposed schlieren and fluorescence image. PLIF image is 30 mm high.

Nitrogen-diluted hydrocarbon-oxygen mixtures are predicted to be most unstable and these show the greatest degree of wrinkling in the shock and OH fronts, with distortions occurring over a wide range of scales (Fig. 2). In the most unstable cases (Austin, 2003, Austin et al., 2005a), separation of shock and OH-front occur and localized explosions in the regions are observed in a high-speed schlieren movie (Fig. 3). They range up to a factor of at least 100 and possibly as high as 1000, and this suggests that there is a type of "turbulent" combustion taking place. The extent to which mixing and diffusion play a role in these mixtures is the subject of ongoing study (Singh et al., 2003).

3 Quantifying the Degree of Regularity

The extent of the geometric complexity is an important issue in determining the roles of the chemical reaction due to chain-branching thermal explosion compared to diffusive transport from the hotter into the colder regions. To gain further insight into the detonation propagation mechanisms, a quantitative analysis of the reaction front complexity was carried out by analyzing

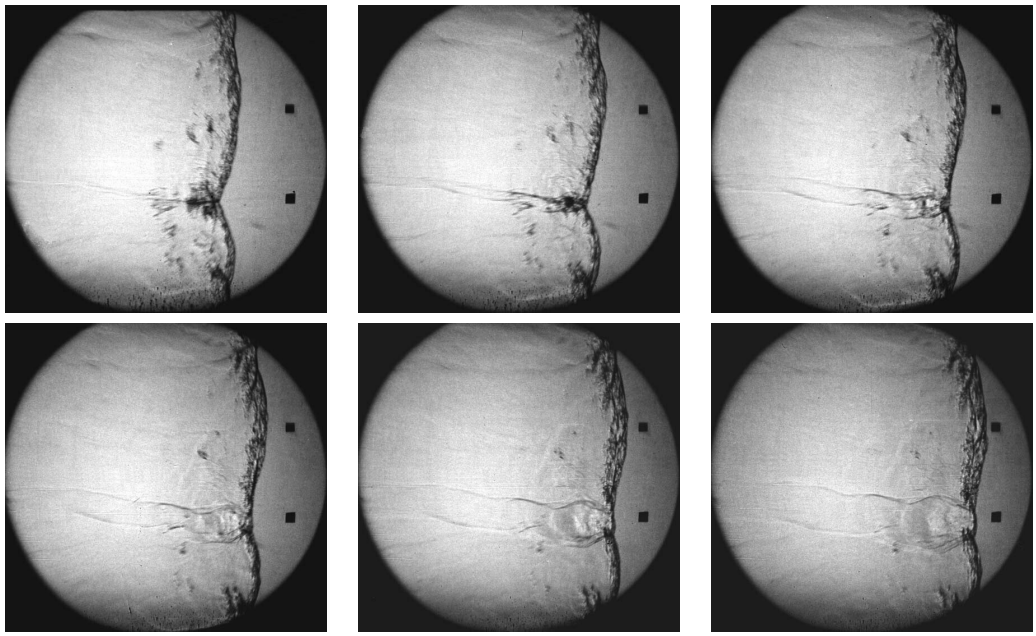

Figure 3: Time-resolved shadowgraph images of a detonation propagating in C_3H_8-$5O_2$-$9N_2$ in the narrow channel. Time between frames is 1.6 μs. Field of view is about 138 mm.

the PLIF images and the imaging system (Pintgen and Shepherd, 2004). The front geometry is characterized by examining two characteristics: the rectified length and the effective dimension. The geometric and the stability characteristics of the mixture are correlated using as a figure of merit the reduced activation energy as computed from detailed chemical reaction mechanisms. The mixtures studied vary in the degree of regularity from "regular" to "highly irregular", corresponding to effective reduced activation energies θ between 5.2 and 12.4. The reaction front outlines were obtained by image processing of the PLIF images (Fig. 4).

It is obvious from visual inspection that the reaction fronts of mixtures classified as "irregular" have a much greater geometric complexity than those of the "regular" mixtures. However, to go beyond this simple observation and make a quantitative analysis of the reaction front geometry requires an evaluation of the imaging system qualities. The key issues are motion blur, modulation transfer function (MTF), light sheet thickness, and image

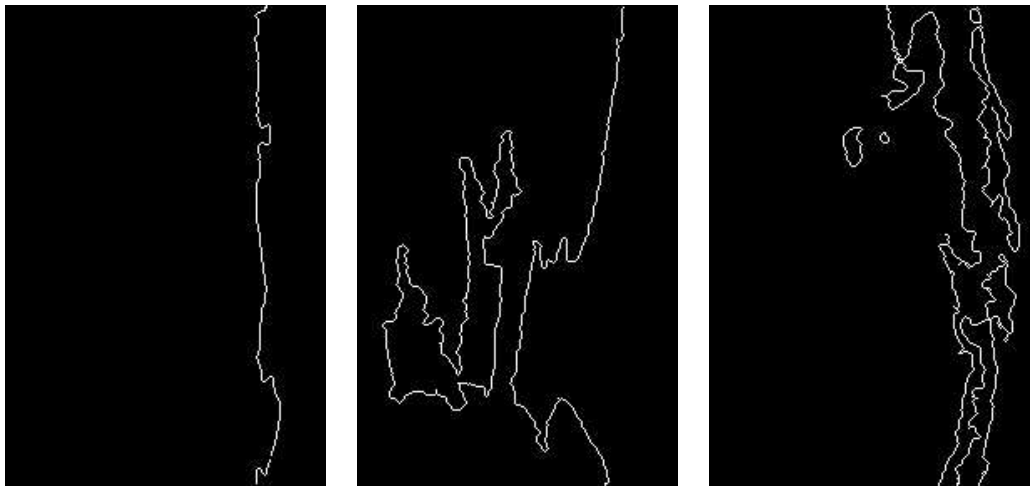

a) $\theta = 5.6$ b) $\theta = 7.8$ c) $\theta = 12.4$

Figure 4: Three examples of edge-detected PLIF images. a) Shot 1653, $2H_2+O_2+17Ar$, image height: 40 mm; b) Shot 1619, $2H_2+O_2+6N_2$, image height: 30 mm; c) Shot 1591, $H_2+N_2O+3N_2$, image height 30 mm.

processing (Fig. 5a). The conclusion from considering all of these effects is that the resolution is not limited by the digital nature of the ICCD but rather by the illumination technique and the degradation of the image due to the contrast reduction resulting from the other optical components, the lens and intensifier. The smallest scale resolvable depends on the image height and ranges from 0.7 to 1.2 mm for images between 30 to 70 mm high (Pintgen, 2004). The normalized edge lengths measured for the "regular" mixtures (Ar-diluted H_2-O_2) range from the minimum of 1 up to 1.8, small compared to the other mixtures studied (Fig. 6a).

For the "highly irregular" mixtures with $\theta = 12.4$, values of normalized edge length up to 7.5 are measured. We have used the box-counting method of fractal analysis to determine an average dimension of the fronts. As for the normalized edge length, a range of dimensions is obtained for each θ. For $\theta \leq 6$, the spread is small and the dimensions range from 1.05 up to 1.15. For the highest value of $\theta = 12.4$, the maximum dimension of 1.5 is obtained (Fig. 6b). The larger maximum values of the dimensions obtained for higher values of θ are quantitative evidence for the increasing degree of corrugation of the reaction front for higher values of θ. Estimates of

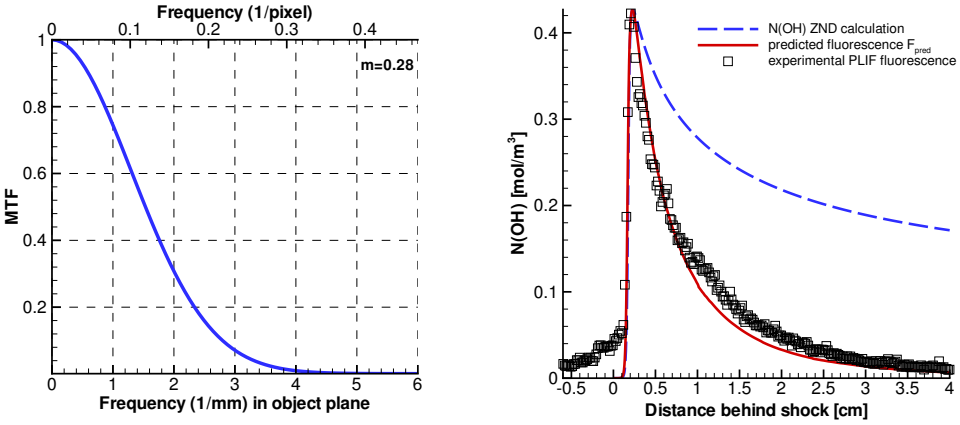

a) b)

Figure 5: a) Modulation transfer function of imaging system, magnification $m = 0.28$. b) Comparison of experimental and predicted fluorescence profile, $2H_2$-O_2-$5.5N_2$, T_0=300 K, p_0=20 kPa.

the three-dimensional reaction surface based on these results are limited by the resolution of the imaging systems, and a definitive conclusion about the possible role of diffusion in the combustion process is not possible at this point.

4 Fluorescence Model

The PLIF technique is used extensively in our laboratory for detonation research (Sections 2, 3 and 5). Up to now, the results have been only qualitative due to the challenges in linking the OH radical concentration to the fluorescence signal. For the conclusive interpretation of the experimentally obtained PLIF images, two key questions were outstanding, both of which were answered by developing a fluorescence model (Pintgen, 2004): Does the location of the fluorescence front seen on PLIF images coincide with the actual OH-concentration front? What is responsible for the strong decay in fluorescence intensity behind the detonation front? The one-dimensional PLIF model predicts the fluorescence intensity profile for a given distribution of thermodynamic conditions and background composition, which were computed with the steady one-dimensional (ZND) detonation structure model. The predicted fluorescence profile was found to be in good agreement with

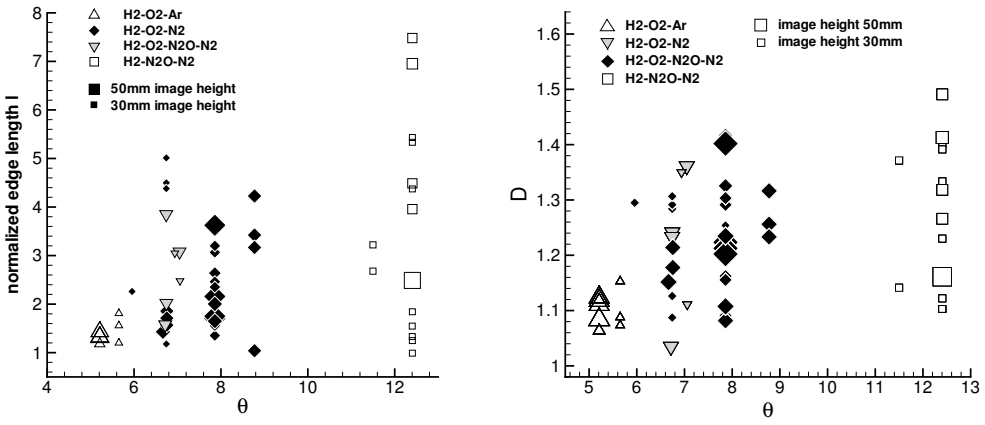

Figure 6: (a) Total edge length as a function of the reduced activation energy θ. (b) Dimension obtained from least-squares linear fit as a function of the reduced activation energy θ. Symbol size scales with height of field of view.

the experimental results (Fig. 5).

The three-level model takes into account light sheet energy absorption (self-absorption by OH and broadband absorption by H_2O and CO_2), broadening and shifting effects on the pumped absorption line, and collisional quenching. The self-absorption of light sheet energy by OH was identified to be responsible for the strong decrease in fluorescence intensity behind the front. This implies that the strong fall-off in fluorescence intensity further behind the front will persist for higher laser output intensities as long as the system operates in the linear fluorescence regime. The absorption effects can be reduced by choosing a weaker transition line for the excitation. This leads to a lower fluorescence signal but a more uniform proportionality constant between fluorescence signal and OH-concentration over the profile. For the current system, this was not achievable since a higher peak fluorescence signal is needed to overcome the noise arising from chemiluminescence. Depending on the mixture, a shift of up to 0.1 mm between the OH-front and the fluorescence front is predicted by the model. This is caused by the strong increase of the collisional quenching during the sharp rise in OH-concentration. For the current work, the results are not affected by this as the scale of the observed structures is larger and the OH-front virtually coincides with the

fluorescence front seen on the PLIF images. For future work, care has to be taken when interpreting fluorescence structures at small spatial scales since the imaging system performance also has to be considered. As also shown in our studies (Section 3), the effective resolution is not only limited by the digital nature of the ICCD but also the modulation transfer function of the imaging system.

5 Detonation Diffraction

The phenomenon of detonation diffraction is important in PDE research as confinement, corners, bifurcating channels, and initiator tubes are present in most realistic PDE design concepts. A further relevant application for detonation diffraction is the exit geometry design (e.g. nozzles) of PDEs. Past studies, also in our laboratory (Schultz, 2000), focused on the critical tube diameter and the development of models for correlating the critical diameter to chemical kinetic and gas dynamic parameters. The goal of the detonation diffraction experiments conducted for the present study is to compare and identify the different patterns and mechanisms observed for decoupling and recoupling of shock and reaction fronts in mixtures with a varying degree of regularity (Pintgen, 2004). The focus is on the failure and re-ignition phenomena occurring in the critical regime. In the critical regime, super- and sub-critical experimental outcomes are possible for nominally identical initial conditions.

Two mixture types, highly diluted H_2-O_2-Ar and H_2-N_2O, were studied in the sub-critical, critical, and super-critical regimes. The mixtures have normalized effective activation energies at CJ conditions of $\theta = 4.5$ and 9.4 respectively, and represent extreme cases in classification of cellular regularity. Different modes have been identified and quantified. Most striking (Fig. 7) were the sub-critical and critical regime, for which the detonation wave fails to transition into the unconfined half-space. For the first time, the reaction front has been directly visualized for a diffracting detonation using PLIF of the OH radical, clearly showing the details of the reaction front.

In the sub-critical case, sawtooth-like geometries in the OH-front are observed where the shock wave decoupled from the reaction front. In the sub-critical case, these structures are passive and much larger in scale than in propagating detonations. In the critical case, the keystone-shaped structures are regenerated by localized explosions. In the super-critical case, the keystones persist and are active as the cellular structure evolves.

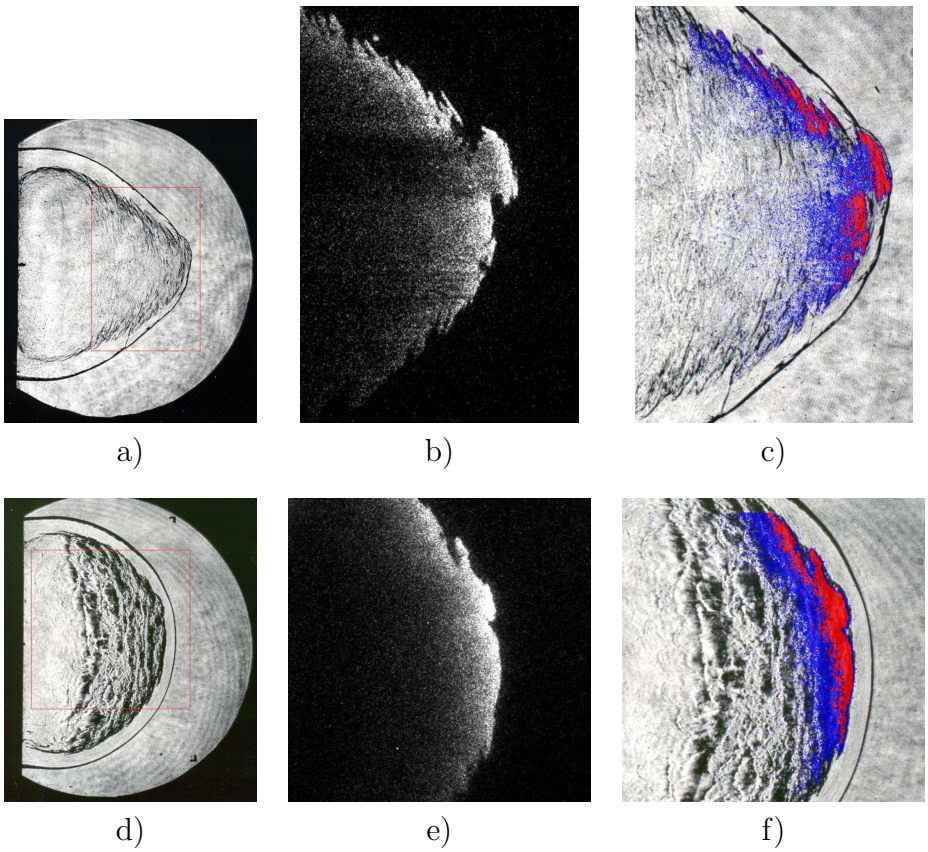

Figure 7: Observations for sub-critical experimental outcome in the critical regime. a), b), and c) 0.22 H_2 + 0.11 O_2 + 0.67 Ar, P_0=100 kPa, $\theta = 4.5$, shot 202. d), e), and f) 0.5 H_2 + 0.5N_2O, P_0=40 kPa, $\theta = 9.4$, shot 80. a) and d) are schlieren images (150 mm height), b) and d) are the simultaneously obtained corresponding OH PLIF images, c) and f) are false color overlays as indicated by boxed region in schlieren images.

For the low-activation-energy mixture and sub-critical outcomes, the reaction front velocity on the center line decays slower than in the high-activation-energy case. In some sub-critical cases, the reaction front was attached to the lead shock up to 2.3 tube diameters from the tube end plate (Fig. 7c). The reaction front velocity was above 0.8 U_{CJ} up to approximately 1.5 tube diameters (d) from the end plate. For the H_2-N_2O mixture, the reaction

front velocity decreased to approximately 0.6 U_{CJ} after a distance of 1.1 d. The whole reaction front decoupled rapidly for the H_2-N_2O mixtures, leading shortly after the tube exit to a self-similar shock shape (Fig. 7d). The rapid decay of the reaction front velocity can be attributed to the higher activation energy of the H_2-N_2O mixture, which leads to large changes in the induction time for small changes in lead shock strength.

A simplified analysis comparing the residence time and the induction time of particles at the OH-front showed that the reaction in the sub-critical case is rapidly quenched with increasing distance from the tube axis. The decoupling is due to rapid increase of induction time relative to residence time as the wave decays. Measurements of the OH-front velocity and shock velocity in the sub-critical case indicate that fluid particles are slowly passing through the OH-front during most of the diffraction event. The shock velocity for the Ar-diluted case decreases more rapidly than in the H_2-N_2O case once the lead shock velocity has reached a velocity below 0.8 U_{CJ}. A sudden decrease is observed for the sub-critical H_2-O_2-Ar case when the lead shock drops below 0.8 U_{CJ}. This can be explained by the rapid increase in the normalized activation energy with decreasing shock velocity for the Ar-diluted mixture. At $U_{shk} = 0.8U_{CJ}$, the normalized activation energy for the Ar-diluted mixture is 35, much higher than the value of $\theta = 16$ for the H_2-N_2O mixture. Clearly, it is important to consider the variation of activation energy with shock velocity and not just the value at CJ conditions.

To reveal the three-dimensional structure of the transverse detonations in the super-critical regime, a stereoscopic image of the high-luminosity region was constructed. This clearly showed the location of the transverse detonation just below the shock surface, which corresponds to the region of high chemiluminescence and high energy-release rate as the transverse detonation travels into the shocked, but unreacted, gas (Fig. 8).

Skews' construction for the propagation of the corner signal into the front was found to be applicable only for the higher activation energy mixture in the sub-critical case. In these cases, the predicted distance at which the corner disturbance signals collide on the tube axis correlates well with the distance at which the reaction front velocity drops significantly. This is due to the fact that, for the higher activation energy, the reaction front decouples very quickly outside the conical area which is not influenced by the corner signal. For the mixture with a lower activation energy, the coupling of reaction front and shock persists longer as changes in the shock velocity have a weaker influence on the induction time.

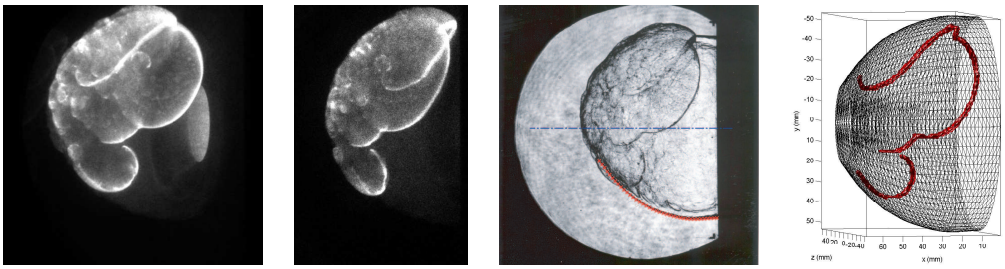

a) b) c) d)

Figure 8: Flow is right to left. a), b) Chemiluminescence images. c) schlieren image with edge-detected decoupled shock. d) Reconstructed transverse detonation with respect to the shock surface.

6 Cycle Analysis and Performance

The application of detonation waves to propulsion was investigated (Wintenberger, 2004) based on thermodynamics and flow path analysis. We observed that the conventional Hugoniot analysis for steady combustion waves, which assumes a fixed initial state and a variable inflow velocity, does not apply for steady-flow propulsion systems. Based on this observation, we reformulated this analysis to obtain a new set of solutions for a fixed initial stagnation state, which we call the stagnation Hugoniot (Wintenberger and Shepherd, 2003c). The implications of the stagnation Hugoniot analysis (Fig. 9a) are that detonations are less desirable than deflagrations for an ideal steady air-breathing propulsion system since they entail a greater entropy rise (Fig. 9b) at a given flight condition. This important result reconciles thermodynamic cycle analysis with past work on detonation-based ramjets, which has systematically concluded that these engines had poorer performance than the ramjet (Dunlap et al., 1958, Wintenberger and Shepherd, 2003b).

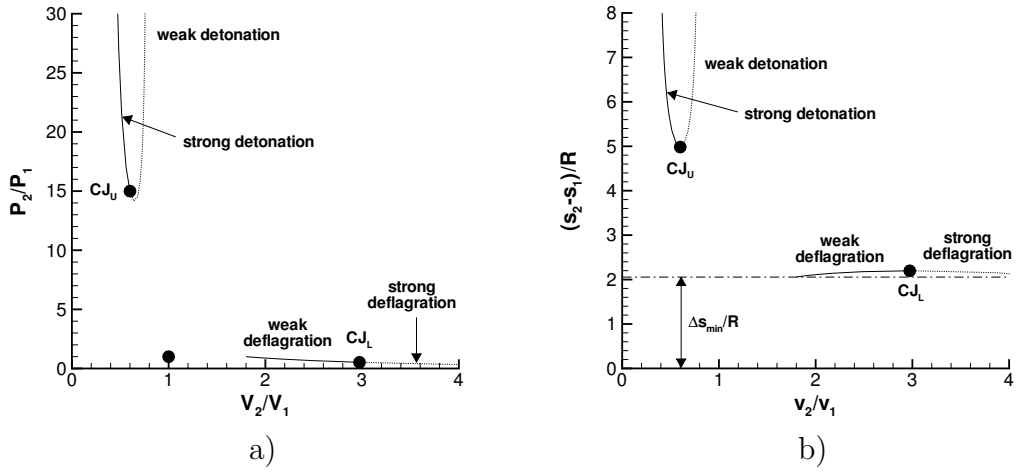

Figure 9: Stagnation Hugoniot in the pressure-specific volume plane (a) and entropy rise (b) along it for a perfect gas.

This leads us to consider the situation for unsteady flow systems. We use a conceptual cycle that we call the Fickett-Jacobs cycle (Jacobs, 1956, Fickett and Davis, 2001) to analyze unsteady detonation waves in a purely thermodynamic fashion. We show that dissociation processes have a strong

influence on the value of the thermal efficiency for real gaseous mixtures. At fixed conditions before combustion, detonations are found to have the potential for generating more work (Fig. 10a) than constant-pressure combustion. The opposite conclusion is drawn when the comparison is made on the basis of the pressure after the combustion process (Fig. 10b). We also find that the thermal efficiency of cycles based on unsteady detonation and constant-volume combustion are very similar. These results are useful in comparing unsteady detonation with other combustion modes. However, these efficiencies cannot be precisely translated into specific performance parameters for unsteady flow propulsion systems (Wintenberger et al., 2003, 2004b,c,a), and we have to rely on flow path analysis to estimate the performance of air-breathing PDEs.

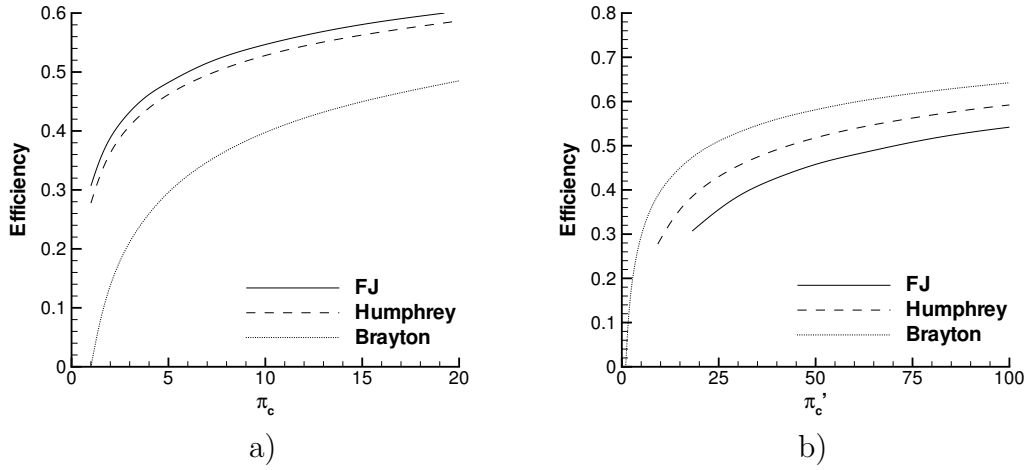

Figure 10: Thermal efficiency as a function of compression ratio (a) and combustion pressure ratio (b) for Fickett-Jacobs (FJ), Humphrey and Brayton cycles for stoichiometric propane-air at 1 bar and 300 K.

Because of the inherent unsteadiness of the flow in PDEs, the most realistic performance models for detonation tubes have so far been based on unsteady gas dynamics. We developed the first complete system-level analysis for an air-breathing PDE. Our analytical performance model for a supersonic air-breathing PDE with a single straight tube (Fig. 11) is based on gas dynamics and control volume methods. It assumes steady inlet flow, large

plenum so that the pressure transients associated with valve opening and closing can be dampened, and infinitely fast valve.

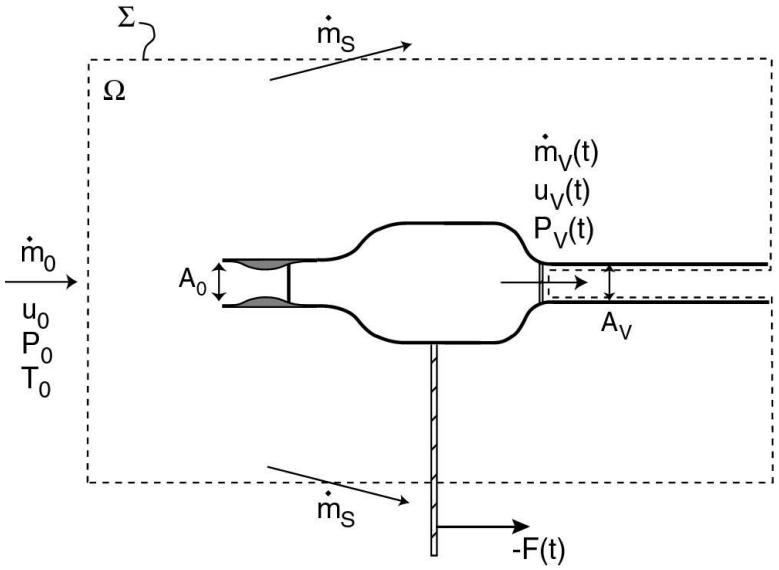

Figure 11: Control volume used for performance analysis of single-tube air-breathing PDE.

The behavior of the flow in the various components of the engine and their respective coupling is modeled for the first time. We show that the flow in the plenum oscillates due to valve opening and closing, and that this unsteadiness results in total pressure losses. We highlight the influence of the interaction between the detonation process and the filling process, which generates a moving flow into which the detonation has to initiate and propagate. Our single-cycle impulse model (Wintenberger and Shepherd, 2003a) is extended to include the effect of filling velocity on detonation tube impulse. Based on this, the engine thrust is calculated using an open-system control volume analysis. It is found to be the sum of the contributions of detonation tube impulse, momentum, and pressure terms. Performance calculations (Fig. 12) for hydrogen- and JP10-fueled PDEs show that thrust is generated up to a flight Mach number of 4 and that the specific impulse decreases quasi-linearly with increasing flight Mach number. We find that PDEs with a straight detonation tube have a higher specific impulse than the ramjet below a flight Mach number of 1.35. PDE performance was found to be very sensitive to the

value of the filling velocity, and potential improvements may be possible with a converging-diverging nozzle at the exit if the pressure in the surrounding atmosphere is low enough so that significant conversion of chemical energy into kinetic energy in the nozzle is possible.

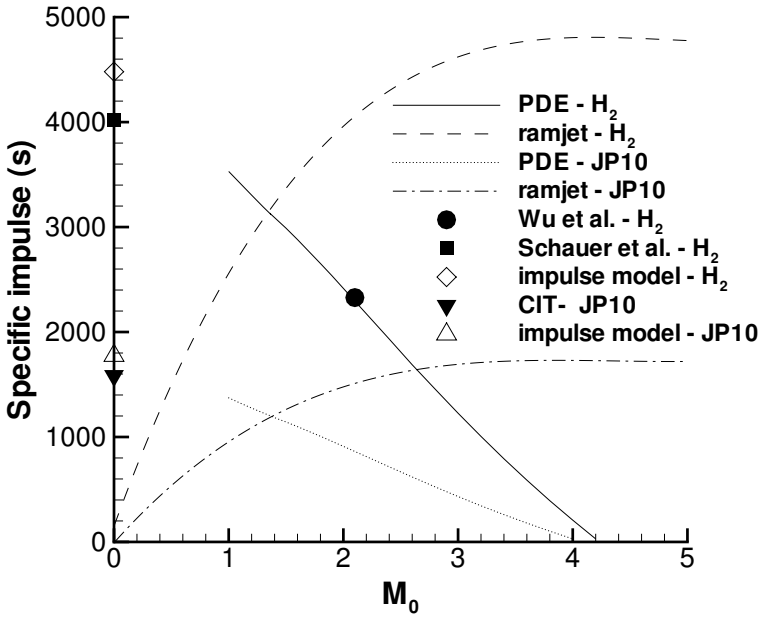

Figure 12: Specific impulse as a function of flight Mach number for a single-tube air-breathing PDE compared to the ramjet operating with stoichiometric hydrogen-air and JP10-air at 10,000 m.

7 Exit Nozzle Study

An experimental and analytical study of impulse generation by detonation tubes has been carried out (Cooper, 2004). It was motivated by the lack of experimental data and scientific understanding on what operating parameters affect impulse. These studies build on our earlier work (Cooper et al., 2002) on measurements of single-cycle impulse in straight tubes. The main topics that are addressed include quantification of the impulse obtained from partially filled tubes operating in atmospheric conditions, fully filled tubes operating in sub-atmospheric conditions, and tubes with exit nozzles.

A new understanding of the mechanisms that lead to the increase in specific impulse when the tube is partially filled has been presented (Cooper, 2004) through new analysis of the detonation tube in terms of the masses and with the development of a "bubble" model that is valid in the limit of a nearly empty tube. Together, these models can be used to correlate the available experimental and numerical data of impulse for a wide range of combustible mixtures and inert gases. In the case of partially filled detonation tubes exhausting into 1 atm environments, previous research (Cooper and Shepherd, 2002, Cooper et al., 2004) determined that the specific impulse increases if only a fraction of the tube contains the explosive mixture. Through analysis of all the available published data, it was determined that a correlation based solely on the volumetric fill fraction (Zhdan et al., 1994, Li and Kailasanath, 2003) does not correctly predict the specific impulse when the densities of the explosive and inert gases are significantly different, such as in the case of hydrogen-oxygen mixtures exhausting into air at standard conditions. Consideration of the principles of energy conservation indicate that the specific impulse depends primarily on the chemical energy of the explosive and the relative mass ratios. Correlation of the specific impulse with the explosive mass fraction was carried out with all the available experimental and numerical data from partially filled detonation tubes (Cooper, 2004). The results (Fig. 13) show that the data can be predicted by a single unifying relationship.

This mass-based relationship clearly fails in the limit when the explosive mass fraction goes to zero because the impulse is dominated by unsteady gas dynamics. An analytical model of an expanding "bubble" of hot, constant-volume combustion products in an infinitely long tube was developed (Cooper, 2004) to successfully predict the theoretical maximum specific impulse from an arbitrary explosive-inert gas combination. The maximum

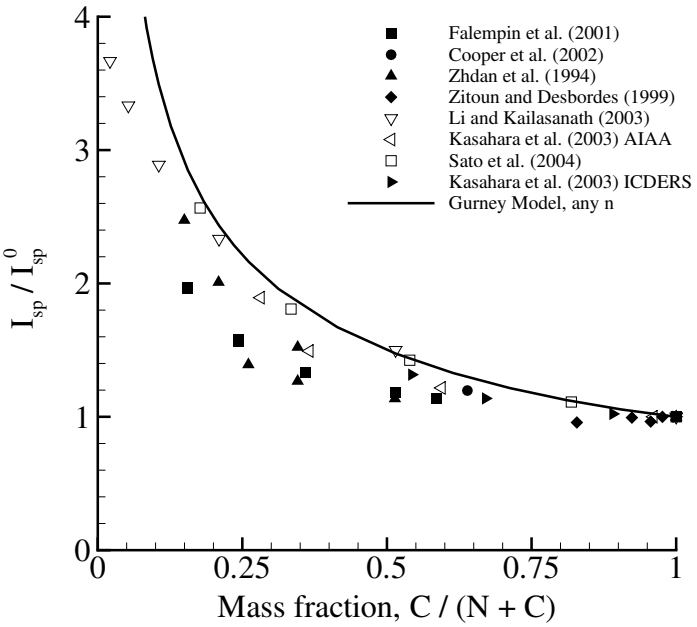

Figure 13: Specific impulse fraction versus mass fraction.

specific impulse was found to depend on the sound speed ratio between the hot expanding products and the inert gas, the ratio of specific heats of the expanding hot products, and the pressure decay at the thrust surface. With one-dimensional gas dynamics, the contact surface trajectory was predicted as the hot products expanded which determined the pressure decay at the thrust surface. A plot of the non-dimensional pressure decay integral was determined for a variety of initial pressure ratios and values for the specific heat ratio in the products. These predictions, along with the new model, are new contributions to the PDE community for which no other models of this kind exist. The predictions are in good agreement with the available numerical data that exists for ethylene-oxygen and hydrogen-oxygen mixtures.

Detonation tubes exhausting into sub-atmospheric pressures were studied (Cooper and Shepherd, 2004b, Cooper, 2004) through the first experimental study directly measuring impulse with the ballistic pendulum as the environment pressure varied. Previously, only a few numerical studies have predicted the impulse under these conditions. The detonation tube was installed within the dump tank of Caltech's T5 hypersonic wind tunnel facility (Fig. 14).

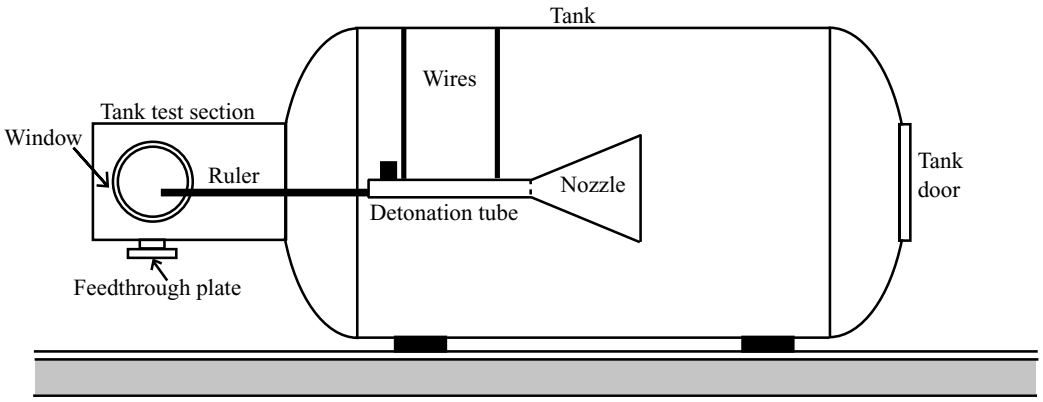

Figure 14: Illustration of detonation tube hung in ballistic pendulum arrangement within Caltech's T5 dump tank (Cooper, 2004).

This enabled tests to be carried out in environment pressures from 100 to 1.4 kPa and with initial pressures between 100 to 30 kPa in the ethylene-oxygen mixtures. The results showed that the impulse increases as the environment pressure deceases. For example, at an initial mixture pressure of 80 kPa, decreasing the environment pressure from 100 to 1.4 kPa increases the impulse by 15%. The increase in impulse is attributed to an increase in the pressure differential across the thrust surface and the blowdown time. With the database of new experimental results, the increase in blowdown time was quantified and used to improve the original impulse model of Wintenberger et al. (2003). The revised model (Cooper, 2004) is capable of accurate predictions of the impulse for a variety of mixtures, initial pressures, equivalence ratios, and, now, for a variety of environment pressures.

The first experiments (Cooper and Shepherd, 2004b, Cooper, 2004) determining the effect of nozzles on detonation tube impulse were also carried out. As before, the impulse was measured as the environment pressure varied, generating the first set of experimental data proving that nozzles can increase the impulse over the case of a plain tube at all sub-atmospheric environment pressures. Previous studies by other researchers have investigated nozzles, but these were carried out with the tube exhausting into 100 kPa air and only a few nozzle designs were tested. A total of twelve different nozzles including converging, diverging, converging-diverging, and a straight extension were tested in this study.

The effect of incomplete product gas expansion is observed when all of the impulse data are plotted in terms of the nozzle pressure ratio P_3/P_0 and compared to the steady-flow impulse predictions assuming isentropic expansion. The straight detonation tube with no exit nozzle generated the lowest values of impulse. Adding a nozzle successfully increases the impulse over the baseline case, yet how the nozzle affects the impulse depends on the pressure ratio.

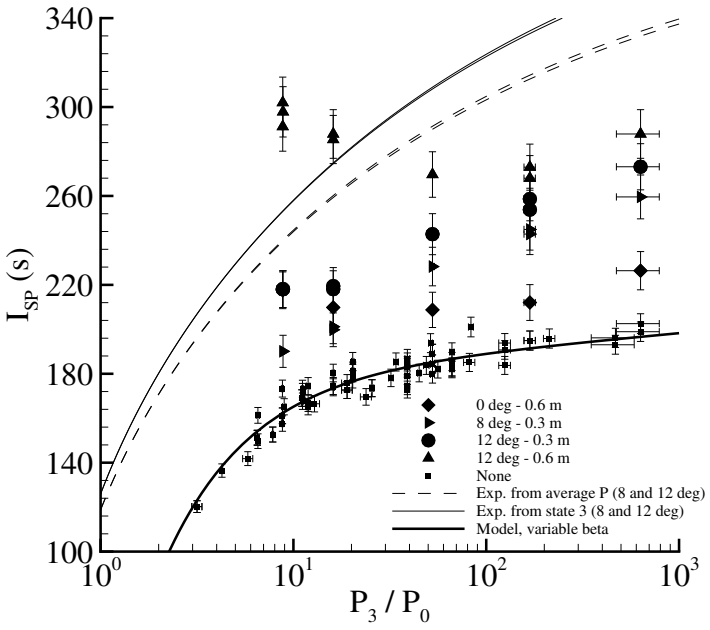

Figure 15: Specific impulse as a function of the nozzle pressure ratio. The steady-flow predictions based on isentropic expansion are also plotted (Cooper, 2004).

Figure 15 is the first demonstration that a nozzle on an unsteady device has two operating regimes. At large pressure ratios, a quasi-steady flow regime is established and the nozzle divergence expands the flow. Here, the impulse values are ordered in terms of increasing nozzle exit area ratio. At small pressure ratios, the unsteady gas dynamics previously investigated in the partially filled detonation tubes are observed. Here, the impulse values are ordered in terms of their mass fractions and are even observed to produce impulse values greater than the steady-flow impulse predictions.

A numerical study (Cooper, 2004, Wintenberger et al., 2004c) was carried out to investigate the effect of chemical non-equilibrium on expanding flows of detonation products by solving the species evolution based on detailed chemical kinetics and a prescribed pressure-time history approximated by the similarity solution for the Taylor wave following a detonation propagating from the closed end of a tube. An eigenvalue analysis of the Jacobian matrix $\mathcal{J}_{ik} = \partial\Omega_i/\partial Y_k$ determined the characteristic time required for the associated progress variables to relax to equilibrium after a disturbance. Comparison of these chemical timescales to the flow timescale (based on the rate of pressure decrease) tested the assumption of chemical equilibrium. Substantial non-equilibrium exists in fuel-air mixtures, especially for particles located near the closed end of the tube. The percentage of the total progress variables that have not equilibrated by the end of the Taylor wave increases as the initial mixture pressure decreases. In a 1 m tube, 20% of the progress variables have not reached equilibrium in the detonation products of a low-pressure ethylene-air mixture, whereas only 4% have not equilibrated in the products of a low-pressure ethylene-oxygen mixture. This means that ethylene-oxygen mixtures can be accurately modeled using the equilibrium flow assumption, but that significant departures from equilibrium are present for low-pressure ethylene-air mixtures, especially in short (< 1 m) detonation tubes.

In addition to the studies on the effect of exit nozzles, partial fill, and ambient pressure, the effect of thrust wall porosity was investigated (Cooper et al., 2003, Cooper and Shepherd, 2004a). A series of single-cycle tests has been carried out to measure the impulse in stoichiometric ethylene-oxygen mixtures initially between 20 and 100 kPa in a detonation tube with a porous thrust surface. The tested thrust surfaces had blockage ratios ranging from completely solid (100% blockage ratio) to completely open (0% blockage ratio). A 76% loss in impulse was observed with a thrust surface blockage ratio of 52% at an initial pressure of 100 kPa. The time to detonation transition was found to be more dependent on the mixture's initial pressure than on the thrust surface blockage ratio. A model of the impulse in detonation tubes with porous thrust surfaces was developed.

8 Detonation Initiators

A detonation initiator has been developed that detonates hydrocarbon-air mixtures using a small amount of hydrocarbon-oxygen gas. This toroidal initiator utilizes shock wave focusing to create a region of high pressure and temperature that is capable of initiating insensitive fuel-air mixtures. In shock wave focusing, this high-energy density region is generated by a converging wave or by the collision of two or more shock waves.

Previous research (Jackson and Shepherd, 2002) developed a prototype toroidal initiator concept. An updated version of the device was used to detonate ethylene- and propane-air mixtures (Jackson et al., 2003). A brief description of the initiator and a summary of current results are presented below. Detailed explanation of the work is available in Jackson et al. (2003) and Jackson (2005).

8.1 Planar Initiator

A planar version of the initiator was built to demonstrate the principles of merging several small wave fronts into a single larger front. The planar initiator is shown in Fig. 16. As with previous designs (Jackson and Shepherd, 2002), the distance from the spark point to the exit plane is identical for each path through the device. Unlike the previous designs, each path has identical flow resistance, ensuring that gas injected at the injection port will evenly fill all of the channels.

Gas is injected into the device through the hole located at the start of the main channel (left of Figure 16). The spark plug (not shown) is located next to this gas injection port. Just downstream of the gas injection port, a series of circular indentations (obstacles) have been milled into the main channel to promote deflagration to detonation transition (DDT). Shortly after the obstacles, the main channel branches multiple times to create a series of channels that exhaust into a test section. The test section is equipped with transducers to measure the planarity of the resulting wave. A polycarbonate window and thin Teflon gasket seal the channels and provide optical access to the top of the initiator. The test section end of the initiator is attached to a longer channel to make Caltech's narrow channel (18×150 mm) test facility (Austin, 2003).

During testing, the initiator and test section are filled with the mixture to be studied. Approximately one second before ignition, equimolar acetylene

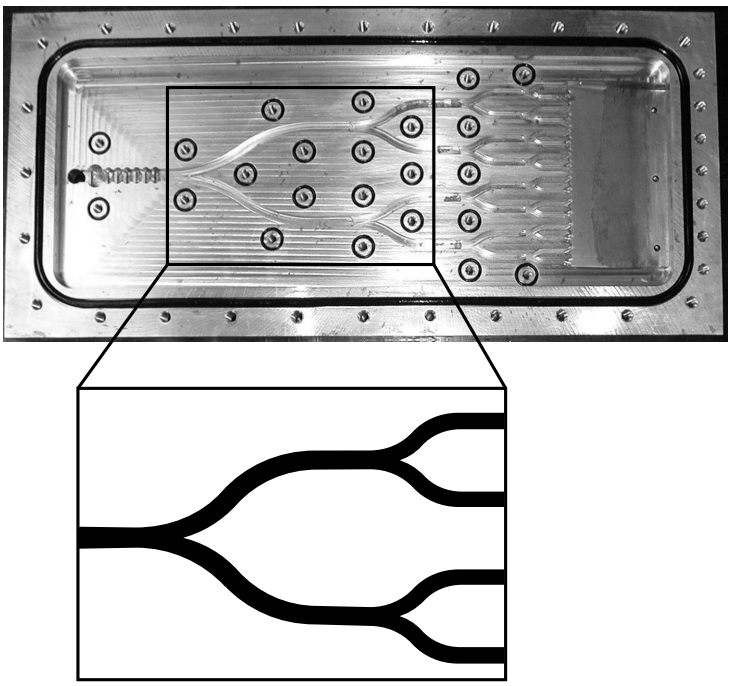

Figure 16: The planar initiator. Note the symmetric channel design.

and oxygen gas is injected into the device through the gas injection port. Injection continues for approximately 0.8 seconds until all initiator channels (but not the test section) are filled with the acetylene-oxygen mixture. When all channels are filled, the spark plug is fired, releasing 30 mJ of stored energy into the initiator mixture. As in the previous design (Jackson and Shepherd, 2002), the resulting deflagration rapidly accelerates into a detonation over the obstacle section in the first channel. The resulting detonation then branches out as it travels down the successive channels. The detonation wavelets emerge at the same time from the small channels into the test section and combine to form a planar detonation, which then propagates through the test section mixture.

Figure 17 contains a series of images taken by an intensified CCD camera with exposure times of 100 ns. The channel orientation is the same as in Fig. 16. Chemiluminescence of the burning gas allows the progress of the detonation to be traced throughout the initiator channels. In the final image, the detonations in the channels have combined in the test section to form the

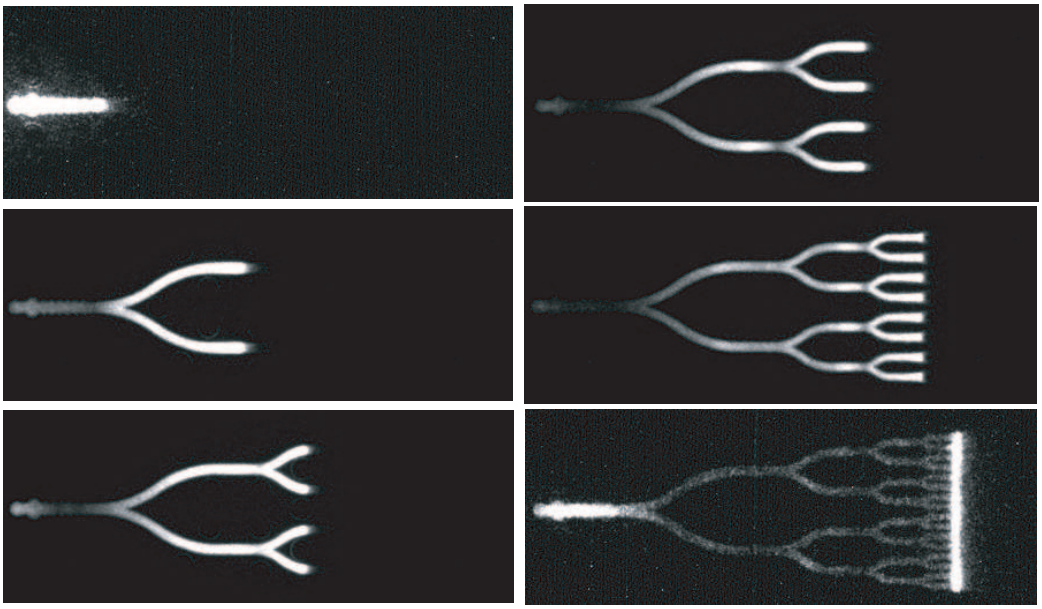

Figure 17: Chemiluminescence imaged from the planar initiator

planar detonation front. Pressure traces from the test section indicate that the resulting front in the test section is planar to within 6 mm over a distance of 15 cm. In addition to acting as a stepping-stone in the design of the toroidal initiator, the planar initiator provides an ideal initiation system to create a large-aspect ratio, planar wave for Caltech's narrow channel facility. Other techniques available to create large-aspect ratio waves use exploding wires or driver tubes. These methods require a large initiator length in order to allow the detonation wave to diffract enough to achieve planarity. The planar initiator provides an equivalent wave in a more compact design.

8.2 Toroidal Initiator

To create the toroidal initiator, the planar initiator design is mapped to the surface of a cylinder. The exit of each channel lies on a circle with the channels exhausting inward (Fig. 18b) to generate an imploding toroidal wave.

The cylinder, or "inner sleeve," containing the channels in the second-generation toroidal initiator is shown in Figure 18a. The inner cylinder con-

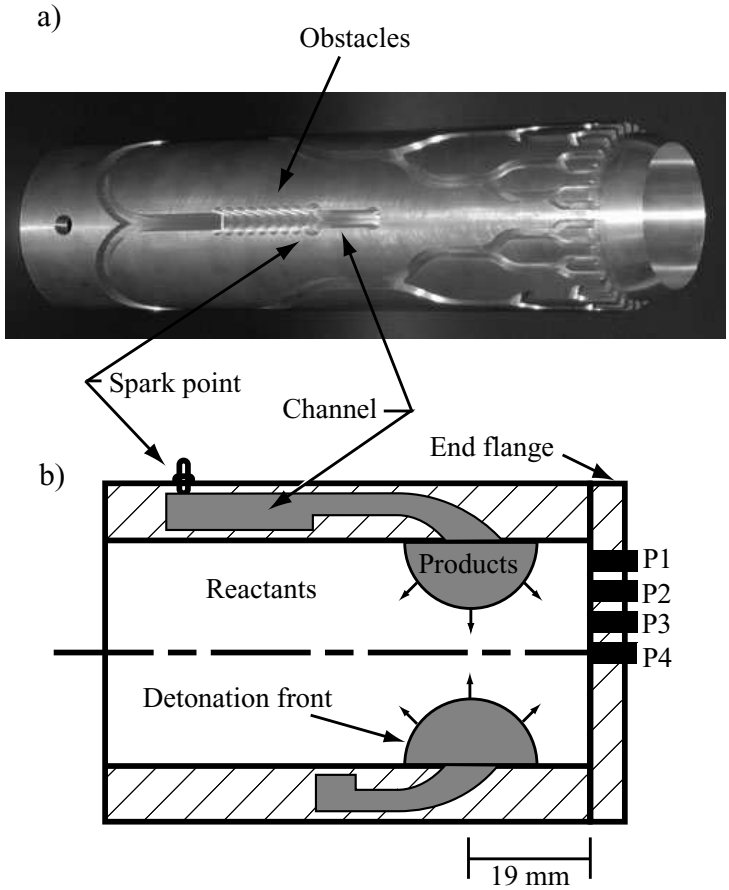

Figure 18: The second generation toroidal initiator a) inner sleeve and b) accompanying schematic. In the schematic, the gray areas are products and the white area is reactants. The hatched sections indicate the initiator walls. Pressure transducers located on the end flange walls are indicated by solid black rectangles.

taining the channels is sealed against an outer sleeve using an interference fit. The inner sleeve was shrunk by immersion in liquid nitrogen and inserted into the cylinder making up the outer sleeve. The dimensions of the cylinders are such that, at room temperature, the outer diameter of the inner sleeve was slightly larger than the inner diameter of the outer sleeve. The result is an interference fit between the two cylinders that acts to seal the channels.

This technique is discussed in Grunthaner et al. (2001).

During initial testing, the toroidal initiator was filled with stoichiometric fuel-oxygen mixtures and the spark was discharged. Pressure transducers at different locations along the end flange and chemiluminescence images showed that the toroidal initiator is capable of generating a repeatable imploding wave with a high-pressure focal region. Pressures near the implosion center were approximately ten times the pressure of a classical Chapman-Jouguet (CJ) detonation wave. Similar focal pressures have also been measured in earlier devices and by other researchers studying cylindrical imploding shock waves (Lee and Lee, 1965).

8.3 Initiation of Hydrocarbon-Air Mixtures

In order to initiate hydrocarbon-air mixtures, the initiator was attached to a longer tube to create a detonation tube 1 m long with 0.4 m composed of the toroidal initiator. The detonation tube was filled with either ethylene-oxygen-nitrogen or propane-oxygen-nitrogen mixtures. After filling the experiment with the insensitive test mixture, an equimolar acetylene-oxygen initiator gas mixture was then injected into the initiator using the same gas injection system used with the planar initiator. Shortly after injection, 30 mJ was discharged across the spark plug. Pressure transducers and ion probes located in the toroidal initiator and detonation tube allowed the resulting wave front to be classified as a detonation or deflagration.

During testing, the amount of diluent in the detonation tube mixture and the amount of gas injected into the initiator were varied. Criteria for successful initiation of the detonation tube mixtures required that wave speeds be not more than 10% below the CJ detonation velocity and that peak pressures be on the order of the CJ pressure in the detonation tube. Additionally, ion probe traces were used to verify that the shock wave measured by the pressure transducers was accompanied by a zone of chemical reaction. Successful detonation initiation of fuel-air mixtures was realized as long as a sufficient amount of initiator gas was injected (Jackson et al., 2003).

The amount of initiator gas used was determined in terms of "initiator overfill," which refers to the amount of gas injected into the experiment that was in excess of the volume of the initiator channels. This initiator overfill is presented as a percentage of the initiator channel volume (349 cc). For example, an initiator overfill value of 0% would correspond to only filling the initiator channels with initiator gas. An initiator overfill value of 100%

would correspond to filling the detonation tube with an amount of gas equal to the volume of the initiator channels.

The wave speeds measured in the detonation tube as a function of initiator overfill are shown in Figs. 19 and 20 for ethylene-air and propane-air mixtures, respectively. From these data, it was determined that the critical amount of overfill is 6% for ethylene-air mixtures and 37% for propane-air mixtures.

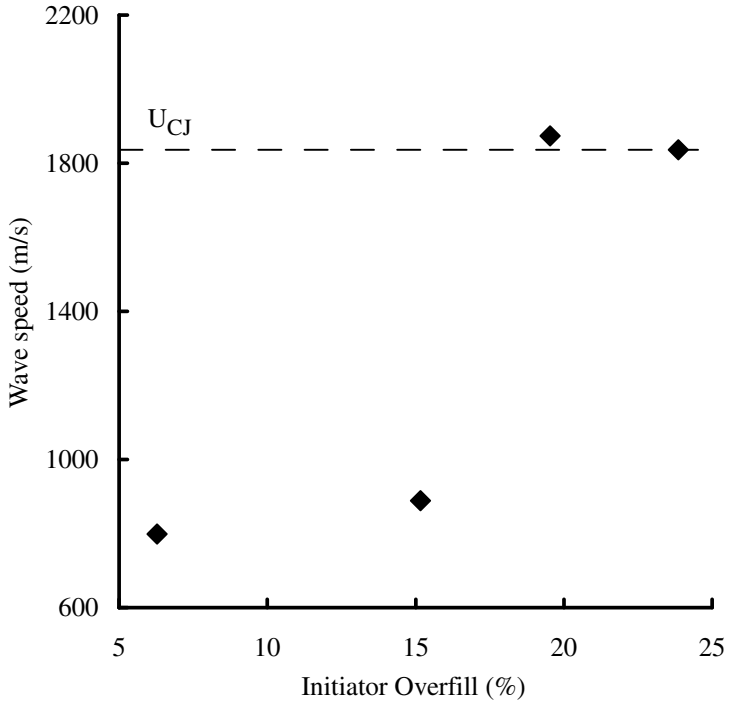

Figure 19: Wave speed in the test section as a function of initiator overfill for stoichiometric ethylene-air mixtures with the focus near the end wall. U_{CJ} is 1825 m/s

Positioning the implosion further from the end flange of the initiator (Fig. 21b) was found to decrease the effectiveness of the imploding wave at initiaton. When the focus was moved 36 cm away from the initiator end flange, higher initiator overfill values were required for initiation. These values are shown in Table 1. The proximity of the end flange to the focus enhanced the initiation process by providing a surface for wave reflection (Jackson, 2005), effectively doubling the size of the initiator.

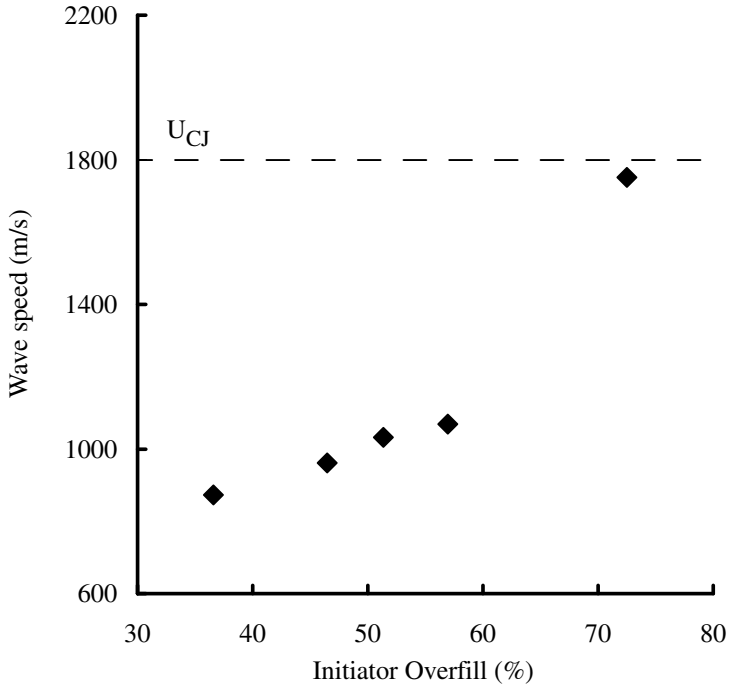

Figure 20: Wave speed in the test section as a function of initiator overfill for stoichiometric propane-air mixtures with the focus near the end wall. U_{CJ} is 1801 m/s

	Near wall	Far from wall
C_3H_8–air	37%	73%
C_2H_4–air	6%	20%

Table 1: Critical amount of overfill necessary for detonation initiation with different experimental configurations.

The energy input to the toroidal initiator was estimated by calculating the energy released by the initiator gas (Jackson et al., 2003). The energy input required for initiation of propane-air was comparable to that used by current initiator tubes when detonating similar mixtures (Murray et al., 2003). However, the toroidal initiator was found to use less oxygen. Also, since the toroidal initiator is incorporated into the walls of the tube, it does not obstruct the flow inside of the tube in the same way as a conventional initiator

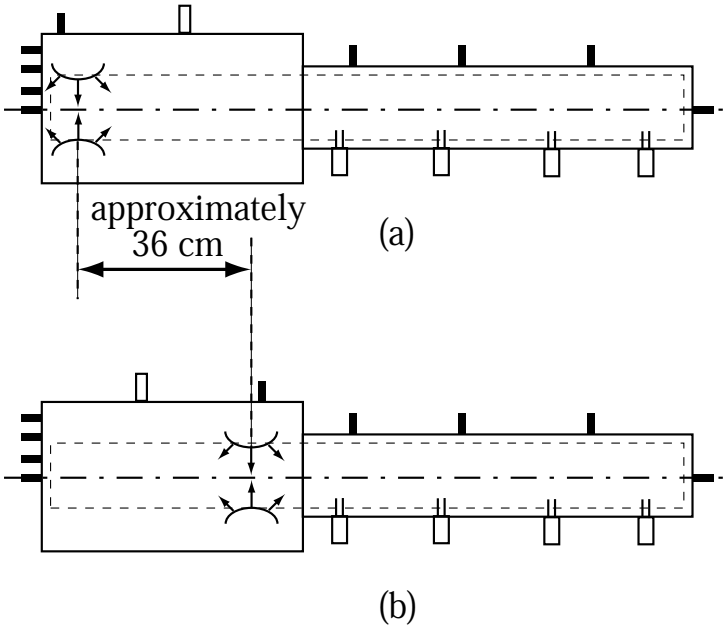

Figure 21: Schematics illustrating the difference in the focal location of the imploding wave when the focus was (a) near the end wall and (b) far from the end wall.

tube and, thus, is an inherently lower drag design with similar effectiveness. Comparison of the imploding detonation wave data to experiments where an imploding shock wave was used for detonation initiation (Jackson and Shepherd, 2004) established that the imploding detonation wave was a more energy-efficient method of initiation. A detailed comparison of the initiator effectiveness to current initiation schemes is available in Jackson (2005).

9 Detonation Initiation via Focusing Reflectors

Detonations and deflagrations were initiated by shock reflection from a parabolic end wall in a tube filled with stoichiometric fuel-oxygen mixtures diluted with nitrogen. Hydrogen, ethylene, and propane were used as fuels. The results (Buraczewski and Shepherd, 2004) determine the critical shock strength necessary to initiate detonations and deflagrations in hydrocarbon mixtures. Mixtures using hydrogen fuel formed a baseline and enabled comparing our experiments to other researchers' studies. The data also provide a comparison to several other types of wave focusing schemes (toroidal imploding detonations and shock waves) used to initiate detonations (Jackson et al., 2003, Jackson and Shepherd, 2004).

Detonation initiation by shock reflection and focusing involves propagating a shock wave into a concave wall. The reflection of the shock from the concave wall will produce a high-energy density focus region with temperatures and pressures in excess of those produced by shock reflection from a flat wall. These high temperatures and pressures promote the initiation of detonation and deflagration.

While detonation initiation with focusing reflectors has been studied by several researchers, much of the work (Chan et al., 1989, Bartenev et al., 2000, Gelfand et al., 2000) has been concerned with hydrogen-oxygen-nitrogen mixtures, which are relatively easy to detonate. Less work (Borisov et al., 1989) is available for hydrocarbon-oxygen-nitrogen mixtures, in spite of the appeal of these fuels for use in current PDE technology. Initiation requirements of propane-air mixtures are of particular interest since they have similar detonation properties to heavier hydrocarbon-air mixtures such as JP10- or JetA-air.

9.1 Experimental Details

Experiments were conducted (Buraczewski and Shepherd, 2004) in a shock tube consisting of three sections: a driver section, a driven section, and a test section. The driver section had a 16.5 cm inner diameter (ID) and was 6.2 m long; the driven section had a 15.2 cm ID and was 11.3 m long. The 2.44 m long test section tube was located at the end of the driven section and had a 7.6 cm ID. An axisymmetric, parabolic reflector was located at the end of the test section. Four different parabolic reflectors were used with four ratios of reflector depth to reflector radius (Fig. 22). The depth-

to-radius ratios tested were 0 (flat wall), 0.5 (shallow), 1.25 (intermediate), and 2 (deep). Pressure transducers and ionization probes located in the test section provided pressure histories and detected the presence of combustion, allowing waves to be classified as nonreactive shock waves, detonations, or deflagrations.

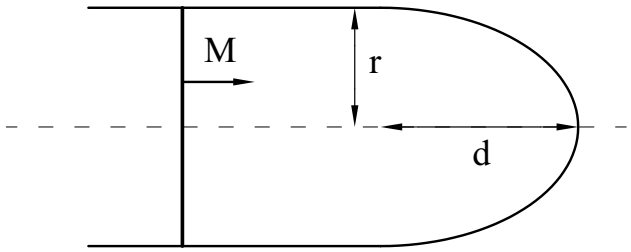

Figure 22: Schematic of a reflector. M is the incident Mach number, r is the radius of the test section tube, and d is the reflector depth. All reflectors were axisymmetric.

A tube with the same ID as the test section protruded 1.94 m into the end of the driven section in a cookie-cutter-style setup which ensured that the shock wave was transferred from the larger-diameter shock tube to the smaller-diameter test section with minimal disruption. The cookie-cutter tube also prolonged the test time of the experiment by extending the duration required for waves reflected from the driven section end flange to enter the test section.

A 12.7 μm thick Mylar diaphragm located between the cookie-cutter and the test section separated the test section gas from the shock tube gas. Compressed air was used in the driver section of the shock tube; nitrogen was used in the driven section. As previously mentioned, the test section gas consisted of stoichiometric fuel-oxygen mixtures diluted with nitrogen. Hydrogen, ethylene, and propane were used as fuels. For each reflector and fuel combination, the incident shock strength and amount of diluent were varied to determine the critical values necessary to initiate detonations and deflagrations at the reflector. The initial pressure of the test section mixture was set such that the pressure behind the reflected wave was approximately 1 bar. This involved varying the initial pressure of the test section mixture from 0.13 bar to 0.73 bar depending on the incident shock strength.

9.2 Results

Four combustion modes were observed during the experiments: detonation initiation inside the reflector, DDT, deflagration initiation outside the reflector, and no combustion. Additionally, for low-nitrogen dilutions, the direct initiation of detonations and deflagrations near the Mylar diaphragm was observed to occur before the incident shock wave reached the reflector. It was concluded that high temperatures resulting from the interaction of the incident shock wave with the Mylar diaphragm were responsible for the premature initiation.

Selected experimental data for ethylene mixtures (Figs. 23 and 24) show the modes of combustion observed in the test section as a function of incident shock Mach number and percent diluent. Each plot is for a specific fuel and reflector combination. Ethylene mixtures were tested with all four reflectors and it was observed that the conditions under which a given mode of combustion occurs are very similar for two sets of reflectors: the two deepest reflectors and the two shallowest reflectors. Hence, only the shallow reflector and the intermediate reflector were used with the propane and hydrogen mixtures.

9.3 Discussion

The results indicate that, as the mixture dilution was increased, the critical Mach number value required for detonation initiation also increased. The highest incident shock Mach number achieved in these experiments was 2.4. Up to this value, detonation initiation inside the reflector was obtained with the intermediate reflector for every mixture tested except for the case of the propane-air (76% nitrogen dilution by volume) mixture. For the shallow reflector, prompt initiation was obtained for hydrogen cases only.

The trend observed was that, for each mixture, there was a minimum Mach number below which no combustion would occur. Mach numbers above the minimum would initiate deflagrations while larger Mach numbers would promote the onset of DDT. Finally, increasing the Mach number even higher would initiate a detonation inside the reflector. Typically, DDT was more prevalent with the flat and shallow reflectors. With the deeper reflectors, the combustion mode was more likely to transition directly from deflagration outside the reflector to detonation inside the reflector.

Additionally, in several situations, combustion was initiated before the

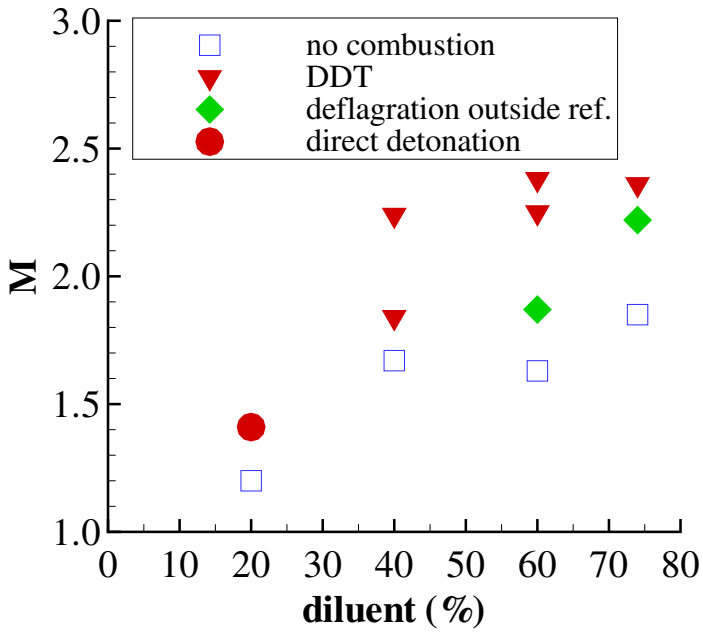

Figure 23: Ethylene-oxygen mixtures diluted with nitrogen tested with the shallow reflector.(Buraczewski and Shepherd, 2004).

incident shock wave reached the reflector. For 20% nitrogen dilution in ethylene mixtures (Figs. 23 and 24), direct initiation of detonation was observed. For 20% nitrogen dilution in hydrogen mixtures, direct deflagration was observed. As previously mentioned, in these cases, the direct initiation was attributed to wave interactions with the Mylar diaphragms.

The two deeper reflectors were found to be more effective at the initiation of detonations and deflagrations via wave focusing. The results obtained for ethylene mixtures indicate no difference between the performance of the intermediate and deep reflectors for detonation initiation. However, reflector depth did affect the minimum Mach number required for deflagration initiation with these two reflectors. Since prompt detonation initiation was not observed during the shallow and flat reflector tests, nothing can be discerned about the effectiveness of these reflectors at promptly initiating detonation.

Comparing the three fuels tested, hydrogen mixtures required the lowest Mach numbers for initiation, and propane mixtures required the highest. For example, in hydrogen mixtures, detonation initiation inside the reflector

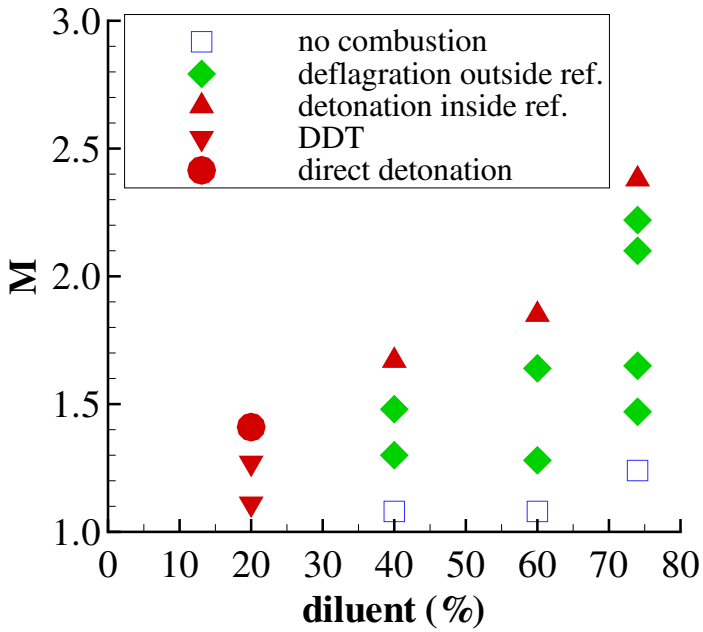

Figure 24: Ethylene-oxygen mixtures diluted with nitrogen tested with the intermediate reflector (Buraczewski and Shepherd, 2004).

occurred with both reflectors tested, while, in the hydrocarbon fuels, this mode of combustion occurred only for the deeper reflectors. Significantly higher Mach numbers were required to cause combustion in propane mixtures than in two other fuel mixtures. During the experiments, the highest incident Mach number used was 2.4, which was not high enough to initiate detonations inside intermediate reflectors for propane-air mixtures. However, applying the trend from the ethylene data to the propane data suggests that an incident shock wave Mach number of approximately 3.5 would be required to initiate propane-air with the intermediate reflector.

10 Corona Discharge Initiator

The transient plasma ignition device developed for detonation initiation at the University of Southern California has been used in various configurations to initiate detonations in static and dynamically filled PDE's (Wang et al., 2004). A high-voltage pulse generator uses a pseudo-spark switch to discharge a capacitor through a transformer connected to electrodes in the initiator. The transient discharge that ensues is in the form of high-energy electron streamers that readily ignite combustible mixtures. In the configuration studied here, the device discharges a couple of joules of energy per pulse. One of the advantages of the plasma initiator is its ability to reduce the residence time of the low-speed combustion stage (Wang et al., 2004). This can benefit PDEs by minimizing the DDT time.

The present study seeks to characterize the effectiveness of the pulsed corona discharge initiator in two ways. The first is to determine its ability to directly initiate detonations in insensitive mixtures as well as in the presence of obstacles. The second is to quantify the reduction in DDT time that would result from minimizing the slow combustive stages of the DDT process. In all cases, a spark plug initiation system is used for the control experiments of this study and the single-cycle tube impulse is measured.

10.1 Characterization of the Corona Discharge Initiator

The pulsed corona discharge initiator makes use of transient plasma as a means of initiation (Liu et al., 2004a). The transient plasma is characterized by radial streamers that occur during the breakdown of the gas. The streamers are a transitional plasma phase (van Veldhuizen and Rutgers, 2002) that lasts for about 50 ns until an arc is formed. Each streamer is comprised of a small streamer head with a large-magnitude electric field and a column of plasma with a low-magnitude electric field. Figures 25a and b are pictures of streamers in a corona discharge and an arc in spark discharge, respectively (Liu et al., 2004b). The pictures illustrate a key difference between the two mechanisms; streamers occur in large numbers that occupy a volume, whereas an arc consists of a single-channel discharge.

The electron energy in a pulsed corona discharge is on the order of 10-20 eV (Marode et al., 1993). This is much closer to the ionization and dissociation levels of many molecules when compared to arc discharge electron

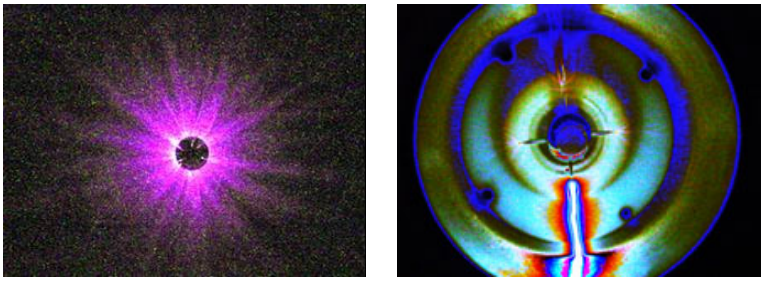

(a) (b)

Figure 25: (a) An image of streamers during a pulsed corona discharge. (b) An image of an arc from a spark discharge. The arc is formed between a needle on the center electrode and the bottom wall of the initiator. It is the overexposed portion of the image. The images are from J. Liu et al., IEEE Transactions on Plasma Science, submitted for publication

energies which are on the order of 1 eV (Liu et al., 2004a).

10.2 Ignition Delay Time

The ignition delay time is plotted in Fig. 26a against % N_2 dilution for the various ignition configurations. The ignition delay time is defined as the time from spark or corona discharge until the first pressure transducer reaches 10% of its maximum value. The figure illustrates that the corona discharge device has roughly a factor of five decrease in the ignition delay time. This persists through the range of nitrogen dilution and ignition configurations tested. The factor of five decrease in ignition time has been previously reported in dynamic fill systems (Wang et al., 2004).

The decrease in ignition time, although important for the practical operation of a PDE, is highly geometry-dependent. In the current experiments, the spark plug was mounted on the initiator flange and combustion wave had to traverse the entire plasma initiator section before it entered the test section where the first pressure transducer was located. This lengthened the ignition delay time compared to the pulsed corona discharge which more readily ignited the entire initiator section volume. It would be more appropriate to compare the pulsed corona ignition delay times to those of a spark plug mounted at the entrance of the test section. Previous (Cooper et al., July,

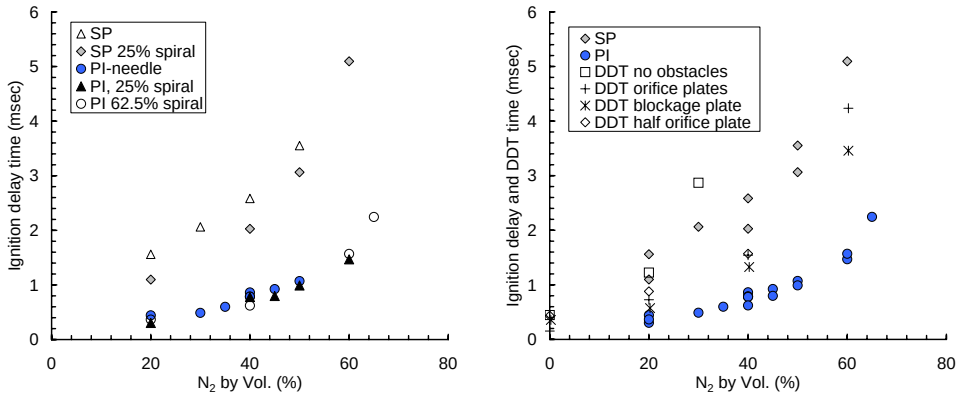

Figure 26: (a) Ignition delay versus % N_2 dilution for the various ignition configurations. (b) Ignition delay and DDT time versus % N_2 dilution for the various ignition configurations. All data in (b) other than SP and PI are from Cooper et al. (July, 2000)

2000) measurements have shown that DDT times for systems with a spark plug mounted at the entrance of the test section were closer to the ignition delay times reported for the pulsed corona initiator. Figure 26b shows the results of this comparison. The DDT times lie in between the plasma initiator and the spark plug times. For clarity, all the spark plug data points and the plasma initiator data points from Fig. 26a have been combined into two groups. The meaning of ignition delay time and DDT time are quite different. The DDT time is the time it takes to record the first detonation observation. The ignition time is the time needed until any disturbance reaches the first pressure transducer. These disturbances are typically detonations or shock waves. The DDT time equals the induction time only if a detonation wave is observed at the first pressure transducer. Therefore, the ignition delay time is a lower bound of the DDT time.

10.3 Comparison of Impulse

A plot of the experimentally determined specific impulse (based on the mixture mass) is shown in Fig. 27a. The specific impulse ranges from 20 s to 160 s depending on the specific mixture composition and initiator-obstacle

configuration. It is observed that at a given nitrogen dilution, the impulse decreases with the increasing blockage of obstacles. This is due to increased drag.

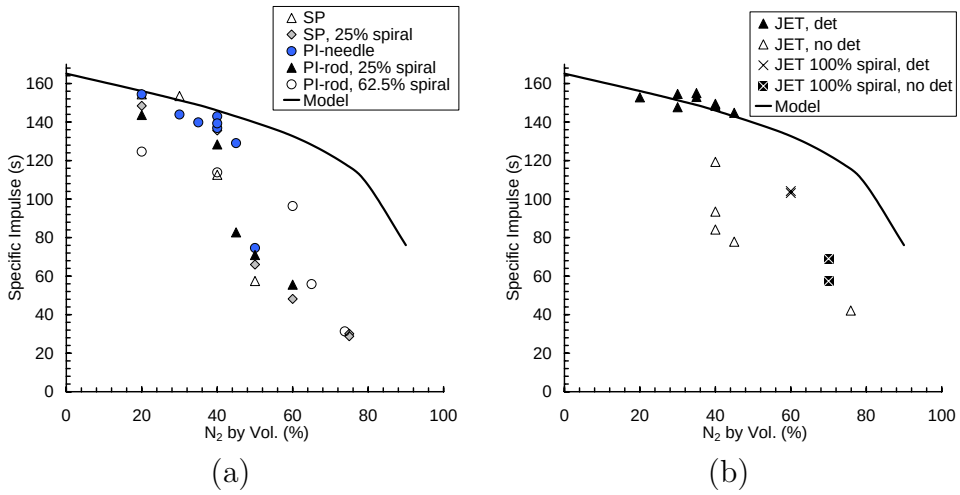

Figure 27: Specific impulse versus % N_2 dilution of stoichiometric ethylene-oxygen mixtures for various initiator-obstacle configurations. SP = spark plug, PI = plasma initiator. Spiral refers to spiral inserts used to promote transition from deflagration to detonation, det refers to observation of a detonation. The model is described in Wintenberger et al. (2003). (a) Experiments in current study. (b) Comparison of impulse in current study with jet initiation data (labeled JET) obtained from Lieberman and Shepherd (2002)

The dramatic drop off in impulse as the nitrogen dilution is increased is a result of a failure to transition to detonation for these mixtures. The solid curve is the impulse predicted by Wintenberger et al. (2003, 2004a) for an ideal detonation. Without the use of obstacles, combustion initiated by the corona discharge can transition to detonation for mixtures with up to 45% nitrogen dilution. A spark plug with no obstacles can initiate combustion that will transition to detonation in mixtures with up to 40% nitrogen dilution. Thus, corona discharge is slightly more effective than a standard internal combustion engine spark plug initiating combustion that will transition to detonation. In all cases, the use of turbulence-generating obstacles significantly improved the effectiveness of detonation initiation as has been found previously (Cooper et al., 2002). Detonations, with the use of obsta-

cles, were observed at up to 65% N_2 dilution in both initiation systems. The corona discharge is effective in achieving very rapid combustion of the region near the electrodes resulting in smaller ignition delay times than arc ignition. Additional means appear to be needed to accelerate the resulting flame to a detonation for mixtures with greater than 40% nitrogen.

Figure 27b compares specific impulse in tests with detonation initiation by means of a turbulent jet (Lieberman and Shepherd, 2002). The turbulent jet was created by combustion of a mixture in a 70 cm^3 chamber connected to the detonation tube via an orifice. The data from the turbulent jet study can be compared to the current data using Figs. 27a & b. The data indicate that the impulse for smooth tube detonation cases agree with the data in the present study and follow the impulse model curve. Above a 45% N_2 dilution, detonations are no longer initiated without the use of obstacles and, thus, the impulse decreases because the combustible mixture gets convected out of the tube by shock or compression waves generated by the deflagration at the initiation end of the tube.

11 Summary

Experimental studies have been carried out on detonation initiation and propagation. Detonations are initiated in tubes and channels using electrical discharges in mixtures of fuel, oxygen, and diluent. Electronic and film imaging systems are used to visualize the density and OH species in detonations, and electronic instrumentation is used to measure flame speed, detonation velocity, and pressure. The ballistic pendulum method is used to study the effect of ambient pressure and nozzles on impulse. Control volume and multi-dimensional numerical simulations are used to predict performance of air-breathing PDEs. The results of each study are summarized below.

Detonation Structure and Narrow Channel Facility. A narrow channel facility has been constructed and over 200 tests have been carried out. PLIF and schlieren (stills and movies) images have been obtained in a variety of mixtures including hydrocarbon fuels typical of pulse detonation engine operation. Highly disturbed fronts were observed with a wide range of length scales and there is evidence of turbulent reaction mechanisms in highly unstable hydrocarbon-air mixtures.

Soot Foil Generation Mechanism. Experimental studies have used our previously developed PLIF method to visualize OH fluorescence while doing simultaneous soot track recording. These measurements demonstrate that the soot tracks are not precisely coincident with the triple points. Experimental studies were also carried out with inert shock wave Mach reflection. Numerical simulations of the wall boundary layer development behind triple points in shock waves demonstrate that wall shear stress variations may be responsible for soot track generation.

Detonation Diffraction Our work on imaging detonation fronts has been extended to study the behavior of fronts during detonation diffraction from a smaller tube to a larger volume. This is a generic situation that is important for detonation initiators, which are based on this principle. The experiments use a 38 mm diameter tube connected to a volume that is 150 $\times$ 150 mm in cross section and 0.6 m long. Pressure measurements, OH PLIF images, laser schlieren images, and multiple-exposure self-luminosity images are used to study how the detonation wave evolves during the diffraction process. A

range of fuel-oxygen-nitrogen mixtures with varying degrees of front instability was studied.

Initiation. Two sets of experiments on initiation were carried out. The first used the toroidal imploding detonation concept and the second used the USC corona discharge initiation system.

The second generation of toroidal initiators was designed, constructed, and tested. The latest design used dynamic injection of the initiator gas to enable testing fuel-air mixtures. The initiation of propane-air mixtures was demonstrated and the performance compared to direct and indirect initiation methods. The effectiveness of the torodial implosion concept was evaluated by comparing the energy content, fuel, and oxygen masses against other direct initiation methods. Limits of N_2 dilution were determined for C_2H_4 and C_3H_8 oxygen mixtures. A related concept of imploding shocks generated by annular jets was tested under a separate contract. The initiation of detonations by shock focusing in paraboloidal reflectors was examined by constructing a special extension to the 6-in shock tube.

Single-cycle impulse N_2 dilution limits were determined for C_2H_4-air mixtures using the ballistic pendulum method and transient plasma discharge initiator developed by Gunderson at USC. Transient plasma discharge is achieved by a high-voltage (90 kV for 50 ns) pulse. The result is a plasma discharge consisting of many radial streamers. A spiral is required to accelerate the flame even with the plasma initiator, and the limiting nitrogen concentration is similar to that observed with a conventional spark plug initiator.

Thermodynamic Models. A control volume model was developed for predicting the performance of an air-breathing engine in supersonic flight. Predictions have been made of specific impulse and thrust specific fuel consumption for hydrogen and JP-10 fuels over a range of flight Mach numbers between 1 and 4 and altitudes up to 10 km. The performance is compared to ramjets and is found to be superior for flight Mach numbers between 1 and about 1.4. A model for steady detonation engines was developed and compared to standard Brayton cycles for ramjets and turbojets. The role of stagnation pressure loss in steady detonation engines is highlighted. Steady detonation-based engines are shown to have a very limited operating range and poor performance relative to the standard Brayton cycles.

Models of steady and unsteady propulsion systems with detonation combustors were developed. For steady propulsion, various combustion modes can be compared by considering an ideal engine in a given flight situation. We have derived the detonation Hugoniot for a fixed upstream stagnation state and shown that the total entropy rise at the CJ detonation point is much larger than for deflagrations. This means that detonations are much less desirable than deflagrations for steady-flow propulsion systems (in agreement with the original argument of Zel'dovich in 1940,) and we also found that the ideal Brayton cycle yields the highest efficiency for an ideal steady-flow propulsion system. The advantage of detonation as a combustion system is possible only for unsteady flow propulsion systems. We have used the ideal Fickett-Jacobs cycle to analyze the unsteady systems and have shown that detonations have the potential to generate more unsteady work than constant-pressure or constant-volume combustion at the same initial pressure, but slightly less at the same final pressure.

Nozzle and Ambient Pressure Effects. Experiments and analysis were completed for the effect of nozzles and low ambient pressure on single-cycle detonation tube impulse performance. Experiments were carried out in a 76 mm diameter, 1 m long tube using the ballistic pendulum method to measure impulse. The tube was located inside a large tank so that the ambient pressure could be varied between 1 and 100 kPa. Conical nozzles and straight extensions were tested. The conical nozzles were found to be effective in significantly increasing the specific impulse at low ambient pressures.

Measurements and analysis of partially filled straight detonation tubes have been reanalyzed and a new model has been developed that better predicts the performance as a function of mass ratio of the filled to unfilled portions. Direct impulse measurements were carried out in ethylene-oxygen mixtures in tubes with and without nozzles in environment pressures between 1.4 and 100 kPa. Impulse with straight extensions increased as P_0 decreased and a new relationship was determined from the experimental data. The mass-based Gurney model and newly developed "bubble model" can be used to predict the impulse of partially filled detonation tubes. Detonation tube nozzles can be used to increase I_{sp} for 100 kPa - 1.4 kPa. Our overall conclusions are that at low pressure ratios (< 100), non-steady gas dynamics and tamping dominate and at high pressure ratios (> 100), quasi-steady isentropic expansion dominates.

References

J. M. Austin, F. Pintgen, and J. E. Shepherd. Lead shock oscillation and decoupling in propagating detonations. 43nd AIAA Aerospace Sciences Meeting and Exhibit, January 10-13, 2005, Reno, NV, AIAA 2005-1170, 2005a.

J. M. Austin, F. Pintgen, and J. E. Shepherd. Reaction zones in highly unstable detonations. In *Proceedings of the 30th Combustion Institute*, number 2, pages 1849–1857, 2005b.

J.M. Austin. *The Role of Instability in Gaseous Detonation*. PhD thesis, California Institute of Technology, Pasadena, California, June 2003.

A.M. Bartenev, S.V. Khomik, B.E. Gelfand, H. Gronig, and H. Olivier. Effect of reflection type on detonation initiation at shock-wave focusing. *Shock Waves*, 10:205–215, 2000.

A.A. Borisov, V.M. Zamanskii, V.V. Kosenkov, and V.V. Lisyanskii. Ignition of gaseous combustible mixtures in focused shock waves. In *Current Topics in Shock Waves, AIP Conference Proceedings*, volume 208, pages 696–701, 1989.

P. M. Buraczewski and J. E. Shepherd. Initiation of detonation by shock focusing. Technical Report FM2004.004, GALCIT, October 2004. Explosion Dynamics Laboratory Report.

C.K. Chan, D. Lau, P.A. Thibault, and J.D. Penrose. Ignition and detonation initiation by shock focusing. In *Current Topics in Shock Waves, AIP Conference Proceedings*, volume 208, pages 161–166, 1989.

M. Cooper, S. Jackson, and J.E. Shepherd. Effect of Deflagration-to-Detonation Transition on Pulse Detonation Engine Impulse. GALCIT, Technical Report FM00-3, July, 2000.

M. Cooper, S. I. Jackson, J. M. Austin, E. Wintenberger, and J. E. Shepherd. Direct experimental impulse measurements for detonations and deflagrations. *Journal of Propulsion and Power*, 18(5):1033–1041, 2002.

M. Cooper, J. Jewell, and J. E. Shepherd. The effect of a porous thrust surface on detonation tube impulse. 39th AIAA/ASME/SAE/ASEE Joint

Propulsion Conference and Exhibit, July 20-23, 2003, Huntsville, Al, AIAA 2003-4822, 2003.

M. Cooper and J. E. Shepherd. The effect of nozzles and extensions on detonation tube performance. 38th AIAA/ASME/SAE/ASEE Joint Propulsion Conference and Exhibit, July 7-10, 2002, Indianapolis IN, AIAA 2002-2628, 2002.

M. Cooper and J. E. Shepherd. The effect of a porous thrust surface on transition to detonation and detonation tube impulse. *Journal of Propulsion and Power*, 20(5):811–819, 2004a.

M. Cooper and J. E. Shepherd. Effect of transient nozzle flow on detonation tube impulse. 40th AIAA/ASME/SAE/ASEE Joint Propulsion Conference and Exhibit, July 11-14, 2004, Ft. Lauderdale, FL, AIAA 2004-3914, 2004b.

M. Cooper, J. E. Shepherd, and F. Schauer. Impulse correlation for partially-filled tubes. *Journal of Propulsion and Power*, 20(5):947–950, 2004.

M. Cooper. *Impulse Generation by Detonation Tubes*. PhD thesis, California Institute of Technology, Pasadena, California, June 2004.

R. Dunlap, R. L. Brehm, and J. A. Nicholls. A preliminary study of the application of steady-state detonative combustion to a reaction engine. *Jet Propulsion*, 28(7):451–456, 1958.

W. Fickett and W. C. Davis. *Detonation Theory and Experiment*. Dover Publications Inc., 2001. Chap. 2, pp. 35–38.

B.E. Gelfand, S.V. Khomik, A.M. Bartenev, S.P. Medvedev, H. Gronig, and H. Olivier. Detonation and deflagration initiation at the focusing of shock waves in a combustible mixture. *Shock Waves*, 10:197–204, 2000.

M. Grunthaner, S.I. Jackson, and J. E. Shepherd. Design and Construction of an Annular Detonation Initiator. Explosion Dynamics Laboratory Report FM01-5, California Institute of Technology, September 2001.

M. P. Grunthaner and J. M. Austin. Design considerations and structural analysis of the narrow channel facility. Technical Report FM2003-003, GALCIT, October 2003. Explosion Dynamics Laboratory Report.

S. I. Jackson, M. Grunthaner, and J. E. Shepherd. Wave implosion as an initiation mechanism for pulse detonation engines. 39th AIAA/ASME/SAE/ASEE Joint Propulsion Conference and Exhibit, July 20-23, 2003, Huntsville, Al, AIAA 2003-4820, 2003.

S. I. Jackson and J. E. Shepherd. Initiation systems for pulse detonation engines. 38th AIAA/ASME/SAE/ASEE Joint Propulsion Conference and Exhibit, July 7-10, 2002, Indianapolis IN, AIAA 2002-2627, 2002.

S. I. Jackson and J. E. Shepherd. Detonation initiation via imploding shock waves. 40th AIAA/ASME/SAE/ASEE Joint Propulsion Conference and Exhibit, July 11-14, 2004, Ft. Lauderdale, FL, AIAA 2004-3919, 2004.

S.I. Jackson. *Detonation initiation via wave implosion*. PhD thesis, California Institute of Technology, Pasadena, California, May 2005.

S. J. Jacobs. The energy of detonation. NAVORD Report 4366, U.S. Naval Ordnance Laboratory, White Oak, MD. Available as NTIS AD113271 – Old Series, 1956.

J.H. Lee and B.H.K. Lee. Cylindrical imploding shock waves. *The Physics of Fluids*, 8(12):2148–2152, 1965.

C. Li and K. Kailasanath. Performance analysis of pulse detonation engines with partial fuel filling. *Journal of Propulsion and Power*, 19(5):908–916, 2003.

D.H. Lieberman and J.E. Shepherd. Detonation initiation by hot turbulent jet for use in pulse detonation engines. In *38th AIAA/ASME/SAE/ASEE Joint Propulsion Conference and Exhibit, Indianapolis, IN, AIAA 02-3909*, July 7-10 2002.

J. Liu, F. Wang, L.C. Lee, N. Theiss, P.D. Ronney, and M.A. Gundersen. Effect of discharge energy and cavity geometry on flame ignition by transient plasma. In *42nd Aerospace Sciences Meeting, 6th Weakly Ionized Gases Workshop*, Reno, Nevada, 5-8 Jan 2004a.

J. Liu, F. Wang, G. Li, A. Kuthi, E.J. Gutmark, P.D. Ronney, and M.A. Gundersen. Transient plasma ignition. submitted for publication, 2004b.

E. Marode, A. Goldman, and M. Goldman. *High Pressure Discharge as a Trigger for Pollution Control*. Ed. by B.M. Penetrante and S.E. Schultheis, Springer-Verlag, Berlin, Germany, 1993.

S.B. Murray, D. Zhang, and K.B. Gerrard. Critical parameters for pulse detonation engine pre-detonator tubes. In *International Colloquium on the Dynamics of Explosions and Reactive Systems*, Hakone, Japan, July 27-August 7, 2003.

F. Pintgen, J. M. Austin, and J. E. Shepherd. Detonation front structure: Variety and characterization. In G.D. Roy, S.M. Frolov, R.J. Santoro, and S.A. Tsyganov, editors, *Confined Detonations and Pulse Detonation Engines*, pages 105–116. Torus Press, Moscow, 2003a.

F Pintgen, CA Eckett, JM Austin, and JE Shepherd. Direct observations of reaction zone structure in propagating detonations. *Combustion and Flame*, 133(3):211–229, 2003b.

F. Pintgen and J. E. Shepherd. Quantitative analysis of reaction front geometry in detonation. In G.D. Roy, A.A. Berlin, S.M. Frolov, J.E. Shepherd, and S.A. Tsyganov, editors, *International colloquium on application of detonation for propulsion*, pages 23–28. Torus Press, Moscow, 2004.

F. Pintgen. *Detonation diffraction in mixtures with various degrees of instability*. PhD thesis, California Institute of Technology, Pasadena, California, December 2004.

E. Schultz. *Detonation Diffraction Through an Abrupt Area Expansion*. PhD thesis, California Institute of Technology, Pasadena, California, April 2000.

S. Singh, D. Lieberman, and J. E. Shepherd. Combustion behind shock waves. Paper 03F-29 Western States Section/Combustion Institute, October 2003.

E.M. van Veldhuizen and W.R. Rutgers. Pulsed positive corona streamer propagation and branching. *J. Phys. D: Appl. Phys.*, 35:2169–2179, 2002.

F. Wang, C. Jiang, A. Kuthi, M.A. Gundersen, C. Brophy, J.O. Sinibaldi, and L.C. Lee. Transient plasma ignition of hydrocarbon-air mixtures in pulse detonation engines. In *42nd AIAA Aerospace Sciences Meeting and Exhibit, AIAA Paper 2004-0834*, Reno, Nevada, 5-8 Jan 2004.

E. Wintenberger, J. M. Austin, M. Cooper, S. Jackson, and J. E. Shepherd. An analytical model for the impulse of a single-cycle pulse detonation tube. *Journal of Propulsion and Power*, 19(1):22–38, 2003.

E. Wintenberger, J. M. Austin, M. Cooper, S. Jackson, and J. E. Shepherd. Erratum to 'comment on analytical model for the impulse of single-cycle pulse detonation tube'. *Journal of Propulsion and Power*, 20(4):765–767, 2004a.

E. Wintenberger, J. M. Austin, M. Cooper, S. Jackson, and J. E. Shepherd. Reply to 'comment on analytical model for the impulse of single-cycle pulse detonation tube'. *Journal of Propulsion and Power*, 20(1):189–191, 2004b.

E. Wintenberger, J. M. Austin, M. Cooper, S. Jackson, and J. E. Shepherd. Reply to 'comment on analytical model for the impulse of single-cycle pulse detonation tube'. *Journal of Propulsion and Power*, 20(5):957–959, 2004c.

E. Wintenberger and J. E. Shepherd. A model for the performance of air-breathing pulse detonation engines. 39th AIAA/ASME/SAE/ASEE Joint Propulsion Conference and Exhibit, July 20-23, 2003, Huntsville, Al, AIAA 2003-4511, 2003a.

E. Wintenberger and J. E. Shepherd. The performance of steady detonation engines. AIAA 41th Aerospace Sciences Meeting, January 2003. AIAA-2003-0714., 2003b.

E. Wintenberger and J. E. Shepherd. Thermodynamic analysis of combustion processes for propulsion. 42nd AIAA Aerospace Sciences Meeting and Exhibit, January 5-8, 2004, Reno, NV, AIAA 2004-1033, 2003c.

E. Wintenberger. *Application of Steady and Unsteady Detonation Waves to Propulsion*. PhD thesis, California Institute of Technology, Pasadena, California, June 2004.

S. A. Zhdan, V. V. Mitrofanov, and A. I. Sychev. Reactive impulse from the explosion of a gas mixture in a semi-infinite space. *Combustion, Explosion and Shock Waves*, 30(5):657–663, 1994.